AD-A247 710

MEASUREMENTS OF LOCAL SKIN FRICTION
IN A MICROBUBBLE MODIFIED TURBULENT
BOUNDARY LAYER

N. K. Madavan, S. Deutsch and
C. L. Merkle

Technical Memorandum
File No. TM 84-136
24 August 1984
Contract N00014-81-C-0481

Copy No. 2

The Pennsylvania State University
Intercollege Research Programs and Facilities
APPLIED RESEARCH LABORATORY
Post Office Box 30
State College, PA 16801

Approved for Public Release
Distribution Unlimited

NAVY DEPARTMENT

OFFICE OF NAVAL RESEARCH

92-07143

92   20   034

REPORT DOCUMENTATION PAGE	READ INSTRUCTIONS BEFORE COMPLETING FORM

1. REPORT NUMBER	2. GOVT ACCESSION NO.	3. RECIPIENT'S CATALOG NUMBER
TM 84-136		

4. TITLE (and Subtitle)	5. TYPE OF REPORT & PERIOD COVERED
MEASUREMENTS OF LOCAL SKIN FRICTION IN A MICROBUBBLE MODIFIED TURBULENT BOUNDARY LAYER	Technical Memorandum
	6. PERFORMING ORG. REPORT NUMBER

7. AUTHOR(s)	8. CONTRACT OR GRANT NUMBER(s)
N. K. Madavan, S. Deutsch and C. L. Merkle	N00014-81-C-0481

9. PERFORMING ORGANIZATION NAME AND ADDRESS	10. PROGRAM ELEMENT, PROJECT, TASK AREA & WORK UNIT NUMBERS
Applied Research Laboratory Post Office Box 30 State College, PA 16804	

11. CONTROLLING OFFICE NAME AND ADDRESS	12. REPORT DATE
Office of Naval Research [Code 432] 800 North Quincy Street Arlington, VA 22217	24 August 1984
	13. NUMBER OF PAGES
	56

14. MONITORING AGENCY NAME & ADDRESS(if different from Controlling Office)	15. SECURITY CLASS. (of this report)
Naval Sea Systems Command [Code NSEA-63R31] Department of the Navy Washington, DC 20362	Unclassified
	15a. DECLASSIFICATION DOWNGRADING SCHEDULE

16. DISTRIBUTION STATEMENT (of this Report)

Approved for public release. Distribution unlimited.
Per NAVSEA - 16 October 1984.

17. DISTRIBUTION STATEMENT (of the abstract entered in Block 20, if different from Report)

18. SUPPLEMENTARY NOTES

19. KEY WORDS (Continue on reverse side if necessary and identify by block number)

skin friction
microbubble
turbulent boundary layer

20. ABSTRACT (Continue on reverse side if necessary and identify by block number)

Local skin friction reductions have been measured using an array of
flush-mounted hot-film probes in a microbubble-modified, zero pressure
gradient, turbulent boundary layer. The results of earlier integrated
skin friction measurements, that showed the reduction to be a function
of plate orientation, gas flow rate and freestream velocity, have been
confirmed both qualitatively and quantitatively. With the measurement

DD FORM 1473 EDITION OF 1 NOV 65 IS OBSOLETE

plate above the boundary layer, it is shown that skin friction is reduced monotonically for all air flow rates at each of three freestream velocities between 4 and 17 m/sec. For the plate below the boundary layer, however, it is possible for increasing gas injection to lead to smaller local skin friction reduction at the lowest speeds. Drag reduction appears to persist for as much as 60-70 boundary layer thicknesses downstream of the injection region. It is further shown, using a probe flush mounted just upstream of the injection section, that there is no apparent upstream interference due to the gas injection. Spectral measurements indicate that microbubbles can cause a reduction of high frequency shear-stress fluctuations. This suggests a destruction of some of the turbulence in the near wall region.

From: N. K. Madavan, S. Deutsch and C. L. Merkle

Subject: Measurements of Local Skin Friction in a Microbubble Modified
               Turbulent Boundary Layer

Abstract: Local skin friction reductions have been measured using an
array of flush-mounted hot-film probes in a microbubble-modified, zero
pressure gradient, turbulent boundary layer. The results of earlier
integrated skin friction measurements, that showed the reduction to be a
function of plate orientation, gas flow rate and freestream velocity, have
been confirmed both qualitatively and quantitatively. With the measurement
plate above the boundary layer, it is shown that skin friction is reduced
monotonically for all air flow rates at each of three freestream velocities
between 4 and 17 m/sec. For the plate below the boundary layer, however, it
is possible for increasing gas injection to lead to smaller local skin
friction reduction at the lowest speeds. Drag reduction appears to persist
for as much as 60-70 boundary layer thicknesses downstream of the injection
region. It is further shown, using a probe flush mounted just upstream of the
injection section, that there is no apparent upstream interference due to the
gas injection. Spectral measurements indicate that microbubbles can cause a
reduction of high frequency shear-stress fluctuations. This suggests a
destruction of some of the turbulence in the near wall region.

I. INTRODUCTION

The authors (Madavan, Deutsch and Merkle 1984a, 1984b; hereafter referred to as MDM1 and MDM2) have recently shown that the introduction of gas bubbles (microbubbles) into a hydrodynamic turbulent boundary layer results in significant reductions in skin friction. In a series of experiments building on some earlier Soviet work (Migirenko and Evseev 1974; Bogdevich and Malyuga 1976; Bogdevich and Evseev 1976), integrated skin friction measurements were made on a 102 mm × 254 mm force balance downstream of a porous injection section. Microbubbles were introduced into the boundary layer by injecting gas (usually air) through the porous surface. The effect of buoyancy, gas flow rate, freestream velocity, gravitational orientation and porous material on the integrated skin friction reduction have been documented in MDM1 and MDM2. Generally speaking, the measurements have shown that the magnitude of the skin friction reduction increases with air flow rate and that it is the ratio of the volumetric flow rate of gas to that of water that is the important parameter. Tests with various types of porous surfaces, including pore size variations over a range of 0.5 to 100 μm, have shown that the skin friction reduction can be realized with a variety of porous materials, although details of the variation of the skin friction reduction with air flow rate are slightly dependent on the type of material.

The microbubble-laden turbulent boundary layer is an extremely complicated flowfield and the mechanisms which lead to the observed skin friction reductions remain unclear. Certainly a proper under-standing of the phenomena cannot be expected from integrated skin

friction measurements alone and calls for the measurement of additional
details of the flowfield. A more precise knowledge of the microbubble
volumetric concentration profiles and bubble size distributions, as well
as the modified mean velocity profiles and corresponding turbulence
characteristics, are necessary prerequisites for achieving such under-
standing. This information, however, is very difficult to obtain. First,
it is noted that the bubble concentrations of interest are quite high
(Migirenko and Evseev 1974 have reported peak concentrations as high as
50 to 80% by volume) so that the microbubble-laden boundary layer is
optically opaque, thus precluding the use of contemporary optical
measurement techniques. Second, both the earlier reported gravitational
effects (MDM1, MDM2) and simple models of the bubble formation process
suggest the phenomenon is operative only at high unit Reynolds numbers.
Thus, the boundary layers of interest are extremely thin, further
aggravating measurement attempts (boundary layer thicknesses are less
than 10 mm, while sublayer thicknesses are a few tens of micrometers in
the current experiments).

Measurements of bubble concentration profiles reported by Migirenko
and Evseev (1974), as well as the authors' own results (MDM1), suggest a
bubble-free layer very close to the wall. Local skin friction measurements
using flush-mounted hot-film probes become then a practical and attractive
first step toward understanding the local characteristics of the micro-
bubble boundary layer. In the current study, an array of flush-mounted
hot-film probes has been used to investigate the downstream evolution and
persistance of the skin friction reduction. The instantaneous signals

from the hot films have also been utilized to compare the spectral content of

the turbulence in the presence and absence of microbubbles.

II. EXPERIMENTAL DETAILS

    (a) Facility and Setup

    The experiments were conducted in the rectangular test section of the

water tunnel facility at The Pennsylvania State University using the boundary

layer on the tunnel test section wall. The tunnel is a closed circuit system

and the rectangular test section has dimensions of 508 mm × 714 mm × 762 mm

long. The flat plate on which the measurements were performed was designed

to replace an existing 279 mm × 533 mm long test section window. A

102 mm × 178 mm long porous section for gas injection, followed by a

102 mm × 254 mm force balance was centered spanwise on this test plate

(see Fig. 1). Details of the facility used and the experimental setup can

be found in MDM1.

    An array of six hot-film probes (TSI 1471W) were employed; five of

these were flush mounted on the force balance downstream of the injection

section, while the sixth probe was mounted immediately upstream. The

locations of the probes are shown schematically on Fig. 2. The probes

were connected to constant temperature anemometers (both DISA 55M01 and

TSI 1750 sets were used). Normally, the probes were operated at an

overheat ratio of 1.06, this value being chosen as a compromise between

probe sensitivity and probe life.

    The porous material used for air injection was of sintered stainless

steel, commercially available for use as filter material. Experiments were

conducted with the smallest available filter material (0.5 μm), as well as

with a larger size (100 μm). The numbers in parentheses refer to the smallest particle size that can pass through the filter, not the actual pore size.

The tunnel test section velocity was monitored by a transducer that measured the pressure drop across the tunnel contraction section. Injected air flow rate and pressure were measured using a flowmeter and a pressure transducer.

(b) Data Acquisition and Run Procedure

Two methods of data acquisition were used. In the initial experiments, the signals from the six hot films were recorded on three Nicolet digital oscilloscopes and stored on floppy disks. The storage capacity of the disks limited these measurements to 2048 points. These digitized signals were then transferred to an IBM 4341 mainframe system for reduction and analysis. Other flow parameters, namely, tunnel freestream velocity, injected air flow rate and pressure, were taken manually from digital voltmeter readouts at the instant the hot-film signals were recorded. In the latter stages of the experiments, an analog-to-digital (A/D) converter was used to digitize the hot-film signals and feed the data directly to an on-line VAX 11/780 computer. Here, the allowable sample size was much larger. For both methods of data acquisition the sampling rate was typically chosen as 2,000 Hz. The minimum record length used was about 1 second. In both procedures, the data channels were sampled sequentially, the maximum delay between the first and last channel sampled being about 10 μs. The instantaneous voltages from the films were recorded and linearization was accomplished on the computer.

The run procedure used for the local skin friction measurements reported here was as follows. The tunnel velocity was held constant and the air flow rate was set at levels ranging from zero to maximum. At each air flow setting, the oscilloscopes were simultaneously triggered (or sampling was initiated on the A/D converter) to record the hot-film signals. Other flow parameters were recorded at the same time the oscilloscopes were triggered. (With the A/D converter, these parameters were also automatically sampled.) Immediately before and after each run with microbubbles, probe calibration runs were performed by recording the hot-film signals over the range of tunnel velocities in the absence of microbubbles.

(c) The Experimental Boundary Layer

The boundary layer into which microbubbles were introduced was documented by measuring the mean velocity and turbulence intensity profiles and stream-wise pressure gradient in the tunnel test section. Details can be found in MDM1, but for the sake of completeness and the important role these data play in hot film probe calibration, the major results are highlighted here.

Mean velocity profiles were obtained at three streamwise locations (shown in Fig. 2) and at two different tunnel speeds (4.7 and 10.6 m/s) using a Laser Doppler Anemometer (LDA). These results are presented in wall variables in Fig. 3, taken from MDM1. The friction velocity used in the figure was evaluated by fitting the near-wall data to Coles (1968) law of the wall. The boundary layer was checked for "full development" by examining the velocity profiles in outer variables, following Purtell et al. (1981). This is shown in Fig. 4, also taken from MDM1. Similarity in the profiles is noted at both tunnel speeds. These velocity measurements, along with measurements of

the pressure gradient along the tunnel test section (see MDM1), establish the

experimental boundary layer as being reasonably close to a classical, fully

developed, zero pressure gradient turbulent boundary layer.

The calibration procedure adopted here for the hot films (as discussed

below) necessitated establishing a virtual origin for the experimental

boundary layer. This was accomplished using the boundary layer displacement

and momentum thicknesses (δ^* and θ), evaluated from the mean velocity profiles

discussed above. Since, for a flat plate turbulent boundary layer, both δ^*

and θ are proportional to the distance from the virtual origin to the 0.8

power (4/5), the latter can be linearly extrapolated from a plot of $\delta^{*5/4}$ and

$\theta^{5/4}$ versus streamwise distance (referenced to a known location along the

boundary layer). By this procedure, the location of the virtual origin was

established 180 mm upstream of the porous injection section, as shown in

Fig. 5.

(d) Skin Friction Probe Calibration Procedure

Flush-mounted hot-film probes relate the heat transfer rate from the

film to the fluid shear stress at the wall. For constant temperature

operation of the film, this relationship between the instantaneous voltage

output by the anemometer, E (which is directly related to the electrical

heat dissipated by the film), and the instantaneous shear stress, τ_w, is

of the form,

$$\tau_w^{1/3} = AE^2 + B \quad . \tag{1}$$

Here A and B are constants that must be determined by a calibration procedure

in a flow where the shear stress is known either from theory or an independent

measurement. Brown (1967), Liepmann and Skinner (1954), and others have

suggested that the constants, A and B, determined from a calibration in a

laminar flow can be used for measurement in a turbulent flow. The validity of

such a procedure has, however, been questioned (see, for example, Bellhouse

and Schultz 1966; Bradshaw and Gregory 1961), since the response of the hot

film in a turbulent flow is not necessarily identical to that in a laminar

flow with the same shear stress. Moreover, it is difficult to obtain a

laminar flow for the calibration experiment, especially one that can cover the

range of shear stress values expected in an actual turbulent flow application

(Ramaprian and Tu 1983). This is particularly true for the high unit Reynolds

number boundary layers of interest here.

In the present study, an in-situ calibration procedure based upon the

verified characteristics of the flat plate turbulent boundary layer was used.

This was accomplished by recording the voltage signals from each probe at a

series of different tunnel freestream velocities in the absence of micro-

bubbles. Each signal record was digitized and stored and the time-averaged

voltage $\bar{E}$ was computed. The mean local skin friction value $\bar{\tau}_w$ at each probe

location and each tunnel velocity was then obtained from classical turbulent

boundary layer correlations of skin friction and length Reyn 'ds number, using

the virtual origin established from the LDA measurements of the velocity

profiles. The use of the classical correlation is justified by the velocity

profile measurements that indicate the present boundary layer is a zero

pressure gradient turbulent boundary layer. The specific correlation used

as the one suggested by White (1974),

$$\bar{\tau}_w = \left(1/2 \rho U_\infty^2\right) \frac{0.455}{\ln^2\left(0.06 \, Re_x\right)} \tag{2}$$

where ρ is the density of water and Re_x the Reynolds number based on the

streamwise length, x, measured from the virtual origin to the probe location.

It is worth noting that at these Reynolds numbers (roughly 2 to 10 million),
a 10% measurement error in virtual origin will result in no more than a 1%
discrepancy in local shear stress.

Having obtained this tabular set of mean voltages and corresponding
values of skin friction, the calibration constants A and B in Eq. (1) are
evaluated by an iterative technique. In this procedure, A and B are initially
approximated by fitting Eq. (1) to the time-averaged tabular data. These
values are then iteratively improved by the method described by Sandborn
(1979a;1979b) and Hanratty and Campbell (1982). In the present study, one
iteration was found sufficient. Two calibration curves were fitted to the
data, one at low and the other at high velocities. A typical calibration
curve is shown in Fig. 6.

It should be emphasized here that the calibration measurements were
made immediately prior to and after measurements with air injection (see
Fig. 6). The average of these two calibrations was used for reducing the
hot-film data in the presence of microbubbles. In cases where the pre-
and post-calibration showed deviations which resulted in the correlation
coefficient of the linear least-squares fit to the data being less than
0.95, the entire data set was discarded.

For the case when there are no bubbles in the boundary layer a measure
of the validity of the hot-film technique can be obtained by comparing the
rms intensity of the skin friction fluctuations, τ'_w, measured here to those
reported in the literature. Mitchell and Hanratty (1966) and Sirkar and
Hanratty (1970) report values of $\tau'_w/\bar{\tau}_w$ ranging between 0.32-0.36 as obtained
from electrochemical shear stress measurments. Eckelmann's (1974)
measurements in the thick viscous sublayer of a glycerine boundary layer

using a flush-mounted hot film provide a value of 0.24. By assuming that very

near the wall $\left(0 < y^+ \lesssim 0.1\right)$ both the streamwise velocity fluctuations u' and

the mean velocity $\bar{U}$ vanish linearly with decreasing distance from the wall,

Eckelmann noted that the value of 0.24 was in agreement with the asymptotic

slope of Laufer's (1950) measurements of $u'/\bar{U}$.

The measured value of $\tau'/\bar{\tau}_w$ in the absence of microbubbles are compared

with the 0.24 value in Fig. 7 for the tunnel velocity range tested. The data

were typically scattered around the value 0.2. The agreement with earlier

results seems quite reasonable, particularly when one considers the difficulty

in obtaining results at the high unit Reynolds numbers and thin sublayers

encountered in this study.

III. RESULTS AND DISCUSSION

Experiments were conducted at tunnel freestream velocities ranging

between 4 and 17 m/s. For the most part, the porous section fabricated from

the smallest available filter material (0.5 μm) was used. Additional experi-

ments were also conducted using the 100 μm porous material. Air flow rates

ranged up to 0.006 m^3/s. As is shown later, this flow rate corresponds to

a volumetric fraction in the boundary layer of about 0.5, assuming that all

of the air flow remains in the boundary layer, which may not be the case.

The local skin friction measurements with microbubbles reported here

are presented in terms of the skin friction coefficient, C_f', normalized to

the corresponding skin friction coefficient without microbubbles, C_{fo}', as a

function of the volumetric fraction of air in the boundary layer. The air

flow fraction was defined as the volumetric flow rate of air divided by the

total flow in the boundary layer

$$\frac{Q_a}{Q_a + Q_w} \tag{3}$$

where

$$Q_w \equiv U_\infty \left(\delta - \delta^* \right) b \quad , \tag{4}$$

and the subscripts a and w denote air and water. The boundary layer thickness

and displacement thickness, δ and δ^*, are obtained from classical correlations

(see White 1974). These thicknesses were calculated at the mid-point of the

porous section (in the absence of microbubbles). The parameter b is the width

of the porous section.

(a) Plate Below the Boundary Layer

The local skin friction measurements at the various hot-film probe

locations with the plate below the boundary layer are shown in Figs. 8

through 10. Note that this orientation (referred to as plate on bottom on

the figures), corresponds to the view shown in Fig. 1, where the experimental

setup is mounted on the bottom wall of the tunnel. The measurements shown

in Fig. 8 are for a tunnel velocity, $U_\infty = 16.7$ m/s, while those in Figs. 9

and 10 correspond to $U_\infty = 10.8$ m/s and $U_\infty = 4.6$ m/s, respectively. The

figures represent measurements using the 0.5 μm porous section. Skin

friction reductions are noted at all tunnel velocities, but the

characteristic trends with volume fraction depend upon U_∞. The reductions

are greatest in the region close to the porous section (probes 2 and 3);

farther downstream, the skin friction relaxes back toward its undisturbed

(no microbubbles) value (probe 6). This is probably due to the decreasing

air content in the boundary layer resulting from both boundary layer growth
and bubble migration. At the high and intermediate tunnel velocities (see
Figs. 8 and 9), the decrease in skin friction is seen to be monotonic with
increasing air flow except possibly for probes 5 and 6 at low air flows.

In contrast to these high and intermediate velocity results, the low
velocity results in Fig. 10 show that the skin friction goes through a minimum
and then increases with increasing air flow. This indicates an optimum air
flow rate for maximum skin friction reduction at low velocities. Based on the
results of Silberman (1957) and Hughes et al. (1979) that indicate the bubble
diameter is proportional to the square root of the ratio Q_a/U_∞, one can
speculate that the reason for this reduced effectiveness of the bubbles at
high air flow rates and low velocities may be due to the larger bubble sizes.
These larger bubbles quickly migrate out of the boundary layer with this plate
orientation, reducing their effectiveness. The same effect was not observed
at the high velocities, apparently because of the shorter convection time.

(b) Plate Above the Boundary Layer

The entire test section of the water tunnel can be rotated through 180
degrees, thus effectively positioning the experimental setup on the upper
wall of the tunnel. At this orientation, the plate is above the boundary
layer (referred to as plate on top in the figures) and the forces due to
gravity act to keep the bubbles in the boundary layer. Earlier reported
force balance measurements (MDM1) showed substantially higher reductions in
the integrated skin friction at this orientation, especially at the lower
velocities. The hot film measurements are shown in Figs. 11 through 13 and
compared to the measurements with the plate below the boundary layer for a

range of tunnel velocities. Figure 11 compares measurements at U_∞ = 16.8 m/s

for the two plate orientations at probe 3 and probe 6 (note that probe 3 is

located close to the injection section and probe 6 is located farthest down-

stream). While the skin friction reductions at probe 3 are of the same

magnitude, slightly larger reductions are noted at the downstream probe

location when the plate is above the boundary layer. Figure 12 is a similar

plot at U_∞ = 10.7 m/s and compares the measurements for the two orientations

at probe 2 and probe 6. Once again, it is noted that close to the injection

section, the skin friction reductions are independent of gravitational

orientation, while farther downstream the plate-on-top orientation again

results in somewhat larger C_f' reductions. These increased reductions with

the plate on top occur because the bubbles remain longer in the boundary layer

where they are most effective. Figure 13 presents additional data for a

tunnel velocity at 4.6 m/s. Note that data for probe 6 with the plate above

the boundary layer are not available. Quantitative comparison between the two

orientations in Fig. 13 is difficult because the maximum air flow rates shown

with the plate above the boundary layer are quite small. The fluctuations in

the hot-film signals at higher air flow rates were very high and, due to the

resulting lack of confidence in the measurments, these results are not

presented. The data, however, suggested that the skin friction reductions

with increasing air flow were monotonic, as compared to the plate-on-bottom

orientation where a definite "bucket" in the curves was noted. These trends

seem reasonable when one notes that the maximum integrated skin friction

reductions reported in MDM1 were observed at this velocity, $(U_\infty$ = 4.6 m/s$)$

with the plate above the boundary layer.

(c) Effect of Pore Size Variations

The size of the microbubbles is certainly an important parameter in the
skin friction reduction. Although both the Soviet results (Bogdevich and
Evseev 1976) and intuition suggest that the pore size would be an important
variable, literature (Silberman 1957; Hughes et al. 1979) on bubble sizes
in turbulent shear flows, though sparse, indicates that the bubble size is
not determined primarily by the size of the pores used for injection, but
by the characteristics of the flow. To investigate this, two widely
different pore sizes, 0.5 μm and 100 μm, were used for gas injection to
compare the magnitude of the skin friction reductions. Figures 14 and 15
compare measurements made using the 100 μm and 0.5 μm porous materials for
the plate below the boundary layer. Figure 14 compares data at probes 2
and 6 at U_∞ = 16.8 m/s. At U_∞ = 10.7 m/s a direct comparison is not
available and for clarity, Fig. 15 presents only the results of the closest
(probe 2) and the farthest (probe 6) locations for the 0.5 μm porous section
(presented earlier in Fig. 9). These data show that injection pore size
does not have a substantial effect on the skin friction results for the
conditions tested here. This observation is in agreement with the integrated
skin friction measurements reported earlier in MDM2. These results are of
some practical importance since with the larger pore size material much less
energy need be expended to introduce a given quantity of microbubbles.

(d) Persistence of the Skin Friction Reduction Phenomenon

The downstream distances to which the skin friction reductions persist
was studied by cross-plotting the data reported above in terms of a non-
dimensional length corrdinate, x/δ, at selected air flow rates. Here x
is the downstream distance measured from the trailing edge of the porous

section and δ denotes the undisturbed boundary layer thickness at this

location. These results are shown in Figs. 16 through 19. The figures

have been reconstructed from mean lines drawn through C'_f/C'_{fo} versus Q_a data.

Figures 16 and 17 are for the plate below the boundary layer, at $U_\infty = 16.7$ m/s

and 10.7 m/s. At both velocities, at low air flow rates, the skin friction

returns to almost its undisturbed value at the downstream probe location

(roughly 35δ). At higher air flow rates, the skin friction reductions are

still significant at this location.

Figures 18 and 19 compare the plate above the boundary layer with the

plate below the boundary layer data at $U_\infty = 16.8$ m/s and 10.8 m/s,

respectively. The persistence is clearly a function of the gravitational

orientation and the tunnel velocity. The slope of the curves is less steep

when the plate is above the boundary layer. Extrapolation would indicate

that the reductions persist even to 60-70δ. This increased effectiveness

is in keeping with other observations.

(e) Upstream Effects due to Introducing Microbubbles in the Flow

In order to check for possible upstream effects of introducing micro-

bubbles into the boundary layer, an additional hot film (probe 1) was mounted

10 mm upstream of the porous injection section. Skin friction measurements at

this location are shown in Fig. 20 as a function of the air flow rate for

several different test runs. The skin friction remains unchanged with air

flow, within the scatter of the data, showing that the introduction of

microbubbles into the flow is not felt upstream over the range of velocities

presented here.

(f) Comparison of Hot Film and Force Balance Measurements

The local skin friction measurements from the array of hot films can be integrated and compared to the force balance results reported in MDM1. The integrations were carried out by subdividing the measurement section into discrete (nonuniform) intervals around each probe location and assuming the skin friction at each section was represented by the measurement at the corresponding probe. Other integration procedures are possible but yield quantitatively similar results (Madavan 1984). The comparisons are shown in Fig. 21 for different tunnel velocities, plate orientations and porous sections. Excellent agreement is noted between the hot films and the force balance measurements. In all cases the maximum discrepancy between the two is less than 10%. This agreement between two measurement techniques that are based on completely different physical principles provides substantiation for both.

(g) Spectral Analysis of Hot Film Signals

The effect of microbubbles on the near wall turbulence structure was studied by extracting frequency information from the hot-film signals. A typical power spectral density function, W(f), defined by the equation

$$\tau'_w = \int_0^\infty W(f)df \quad ,$$ (5)

where f is the frequency in cycles per second, is presented in inner variables for no air injection in Fig. 22. The data is from probe 2 and the plate is on the bottom; the different symbols represent various velocities ranging between 4.0 and 17.0 m/sec. The collapse of the data is quite good.

The influence of the microbubbles may be most strikingly observed by considering a sequence of hot-film signal traces comprising a typical run (probe 3, 16.8 m/sec, plate on bottom) as shown in Fig. 23. The traces have been redrawn from the digitized, linearized signals as processed by the computer. The drop in the mean level of skin friction as the air flow rate is increased from zero is clearly seen with reference to a fixed skin friction value, τ_{ref}. In the presence of microbubbles, the hot-film signals exhibit a reduced amount of high frequency content and the turbulence energy appears to shift toward lower frequencies.

In Figs. 24 and 25 the power spectral density functions with microbubbles for probe 2 at a free stream speed of 10.7 m/sec are shown in inner variables. Figure 24 is for the plate below the boundary layer while Fig. 25 is for the plate above. Note that u_τ and τ'_w used in these normalizations are the values with air injection, so that the loss of high frequency signal is masked by the scaling. The inner variable scaling thus remains effective for the micro-bubble boundary layer. Similar results are observed at higher speeds as shown in Fig. 26. These correspond to the signal traces previously presented in Fig. 23 (probe 3, 16.8 m/sec, plate on bottom).

The power spectral density functions indicate, by the success of inner variable scaling, that the introduction of air causes no major restructuring of the turbulent boundary layer. We note that there is a strong similarity between the results presented here and those obtained in the polymer flow of Fortuna and Hanratty (1972). Apparently there are some similarities in the drag reduction mechanisms for polymers and microbubbles.

IV. CONCLUDING REMARKS

An array of flush-mounted hot films has been used to study the downstream evolution and persistence of the skin friction reduction in the microbubble-laden turbulent boundary layer. The measurements with the hot films are in excellent agreement with earlier reported integrated skin friction measurements obtained using a force balance. The downstream persistence of the skin friction reduction beyond the location of microbubble injection is a function of the gravitational orientation of the plate and the freestream velocity. For the plate above, the boundary layer substantial skin friction reduction persist for some 35δ for low air flow rates and up to $60-70\delta$ for high air flows. The reductions persist for somewhat shorter distances, roughly 50δ, for the plate below the boundary layer.

Contrary to earlier Soviet results, injection pore size was found to have no major effect on the amount of skin friction reduction. A hot-film probe located 10 mm upstream of the porous injection section indicates that gas injection causes no significant upstream influence for the range of freestream speeds tested.

Spectral measurements indicate a clear loss of high frequency signal with air injection. Inner variable scaling of the spectra with u_τ and τ_w', however, seems as effective with microbubbles as without. This indicates that the major effect of the microbubbles in the turbulent boundary layer may be to alter the local effective viscosity and density of the fluid, thus changing the local turbulent Reynolds number, rather than introducing a major restructuring of the turbulence.

ACKNOWLEDGMENT

REFERENCES

Bellhouse, B. J. and Schultz, D. L. 1966. Determination of Mean and Dynamic
Skin Friction, Separation and Transition in Low Speed Flow with a Thin
Film Heated Element. J. Fluid Mech. 24, p. 379.

Bogdevich, V. G. and Evseev, A. R. 1976. Effect of Gas Saturation on Wall
Turbulence. In Investigations of Boundary Layer Control (in Russian)
(eds. S. S. Kutateladze and G. S. Migirenko), p. 49. Thermophysics
Institute Publishing House.

Bogdevich, V. G. and Malyaga, A. G. 1976. The Distribution of Skin Friction
in a Turbulent Boundary Layer of Water beyond the Location of Gas
Injection. In Investigations of Boundary Layer Control (in Russian)
(eds. S. S. Kutateladze and G. S. Migirenko), p. 62. Thermophysics
Institute Publishing House.

Bradshaw, P. and Gregory, N. 1961. The Determination of Local Turbulent Skin
Friction from Observations in the Viscous Sublayer. Aero. Res. Counc.
R. & M. 3202.

Brown, G. L. 1967. Theory and Application of Heated Films for Skin Friction
Measurements. Proc. 1967 Heat Transfer and Fluid Mech. Inst. p. 361.
Stanford University Press.

Coles, D. E. 1968. The Young Person's Guide to the Data. Proc. AFOSR-IFP
Stanford Conference on Computation of Turbulent Boundary Layers.
(eds. D. E. Coles and E. A. Hirst). Stanford University Press.

Eckelmann, H. 1974. The Structure of the Viscous Sublayer and the Adjacent
Wall Region in a Turbulent Channel Flow. J. Fluid Mech. 65, p. 439.

Fortuna, G. and Hanratty, T. J. 1972. The Influence of Drag-Reducing Polymers
on Turbulence in the Viscous Sublayer. J. Fluid Mech. 53, p. 575.

Hanratty, T. J. and Campbell, J. A. 1982. Measurement of Wall Shear Stress.
In Fluid Mechanics Measurements (ed. R. J. Goldstein). Hemisphere
Publishing Corporation.

Hughes, N. H., Reischmann, M. M. and Holzmann, J. M. 1979. Digital Image
Analysis of Two Phase Flow Data. 6th Bienn. Symp. on Turbulence,
University of Missouri, Rolla.

Laufer, J. 1950. Investigation of Turbulent Flow in a Two Dimensional
Channel. NACA Rept. TN 2123.

Liepmann, H. and Skinner, G. 1954. Shearing-Stress Measurements by Use of
a Heated Element. NACA TN 3268.

Madavan, N. K., Deutsch, S. and Merkle, C. L. 1984a. Reduction of Turbulent
Skin Friction by Microbubbles. Phys. Fluids 27, p. 356.

Madavan, N. K., Deutsch, S. and Merkle, C. L. 1984b. The Effect of Porous
Material on Microbubble Skin Friction Reduction. AIAA Paper 84-0348.

Madavan, N. K. 1984. The Effects of Microbubbles on Turbulent Boundary
Layer Skin Friction. Ph.D. Thesis, Dept. of Mech. Engr., The
Pennsylvania State University.

Migirenko, G. S. and Evseev, A. R. 1974. Turbulent Boundary Layer with Gas
Saturation. Problems of Thermophysics and Physical Hydrodynamics
(in Russian). Novosibirsk, Nauka.

Mitchell, J. E. and Hanratty, T. J. 1966. A Study of Turbulence at a
Wall using an Electrochemical Wall Shear Stress Meter. J. Fluid
Mech. 26, p. 199.

Purtell, L. P., Klebanoff, P. S. and Buckley, F. T. 1981. Turbulent Boundary
Layer at Low Reynolds Number. Phys. Fluids 24, p. 802.

Ramaprian, B. R. and Tu, S. W. 1983. Calibration of a Heat Flux Gage for

    Skin Friction Measurement. J. Fluids Engr. 104, p. 455.

Sandborn, V. A. 1979a. Surface Shear Stress Fluctuations in Turbulent

    Boundary Layers. Second Symposium on Turbulent Shear Flows.

    Imperial College, London, p. 361.

Sandborn, V. A. 1979b. Evaluation of the Time Dependent Surface Shear

    Stress in Turbulent Flows. ASME Preprint 79-WA/FE-17.

Silberman, E. 1957. Production of Bubbles by the Disintegration of Gas

    Jets in Liquid. Proc. 5th Midwestern Conf. on Fluid Mech.,

    University of Michigan, p. 263.

Sirkar, K. K. and Hanratty, T. J. 1970. The Limiting Behavior of the

    Turbulent Transverse Velocity Component Close to a Wall. J. Fluids

    Mech. 44, p. 589.

White, F. M. 1974. _Viscous Fluid Flow_. McGraw-Hill Publishing Co.
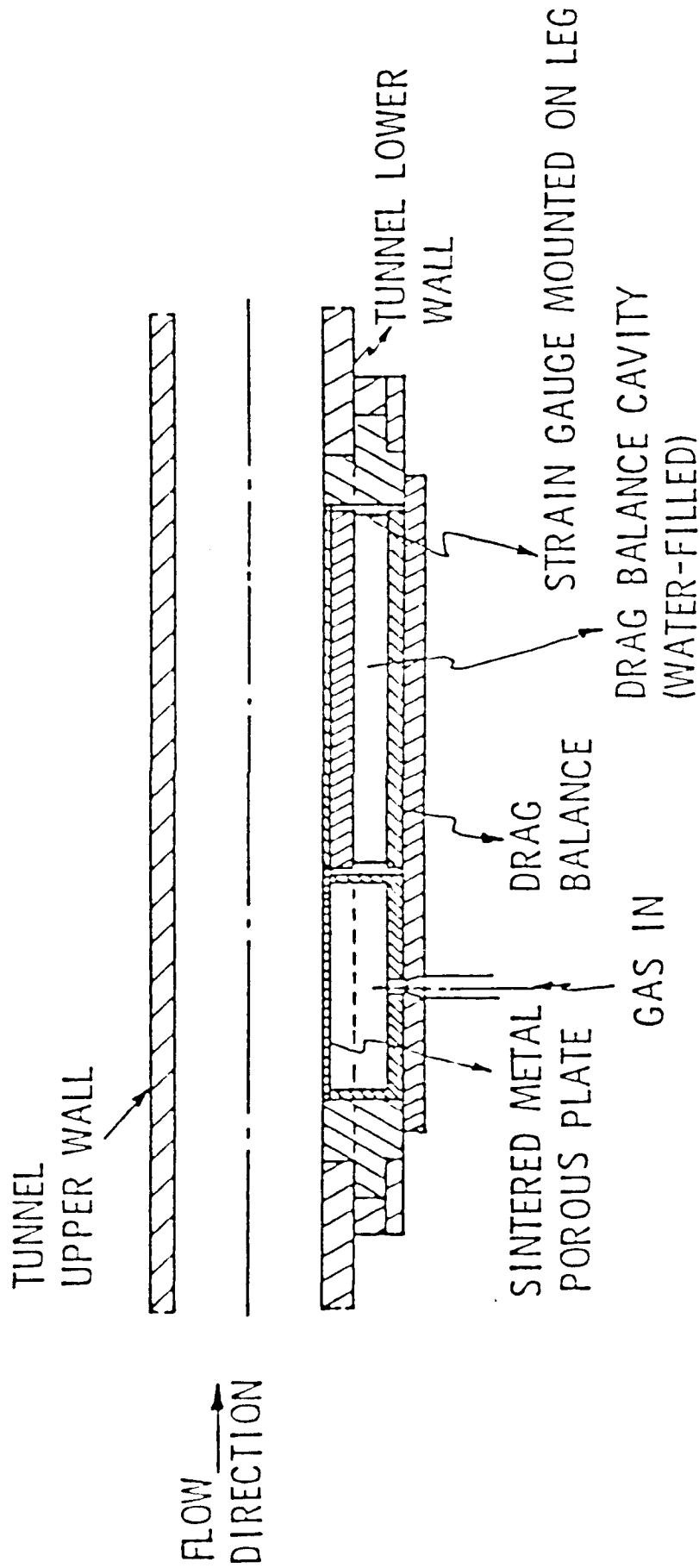
FIGURE CAPTIONS

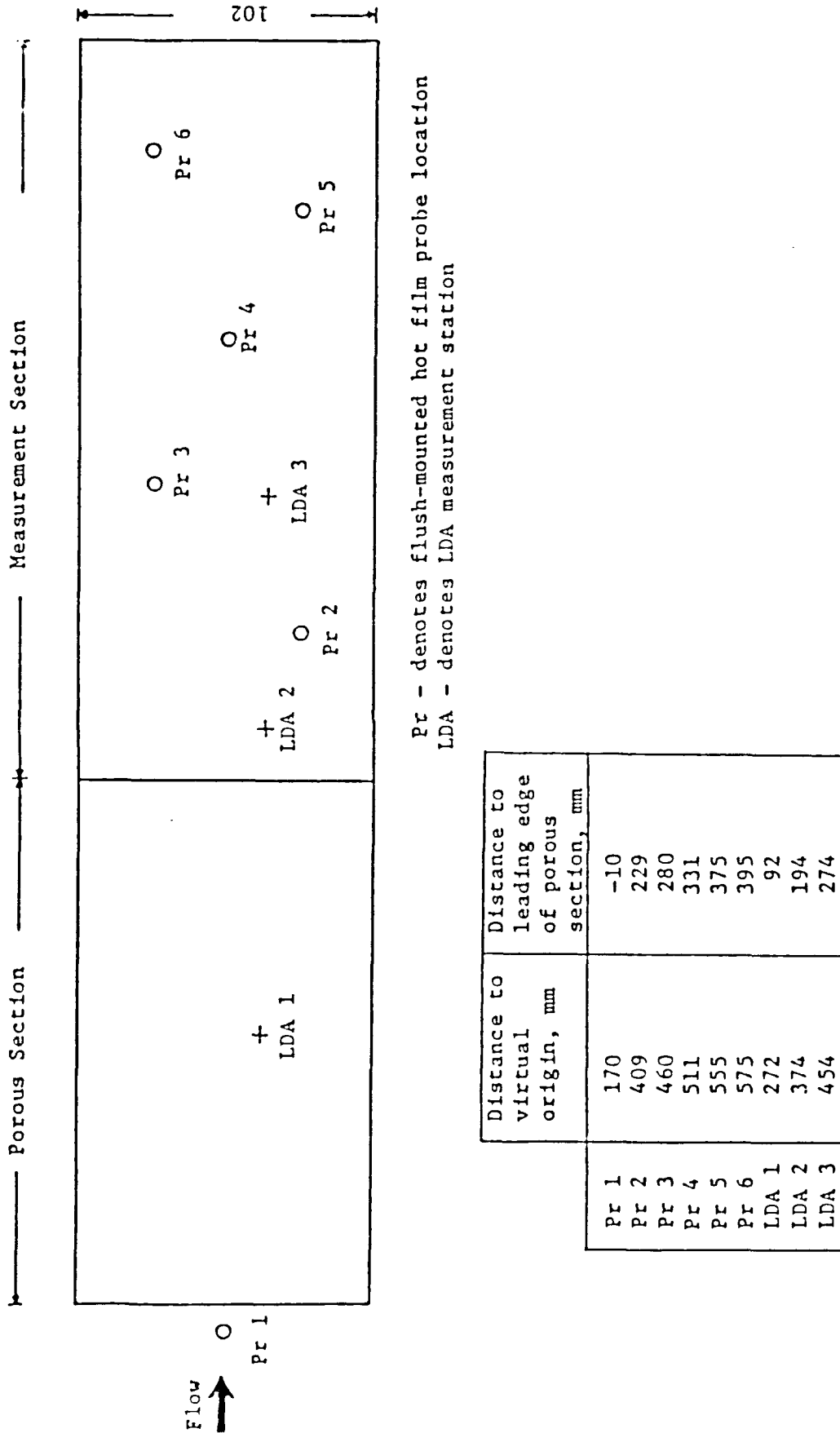Figure 1.   Schematic of an experimental setup.

Figure 2.   Schematic showing hot film probe locations and LDA measurement
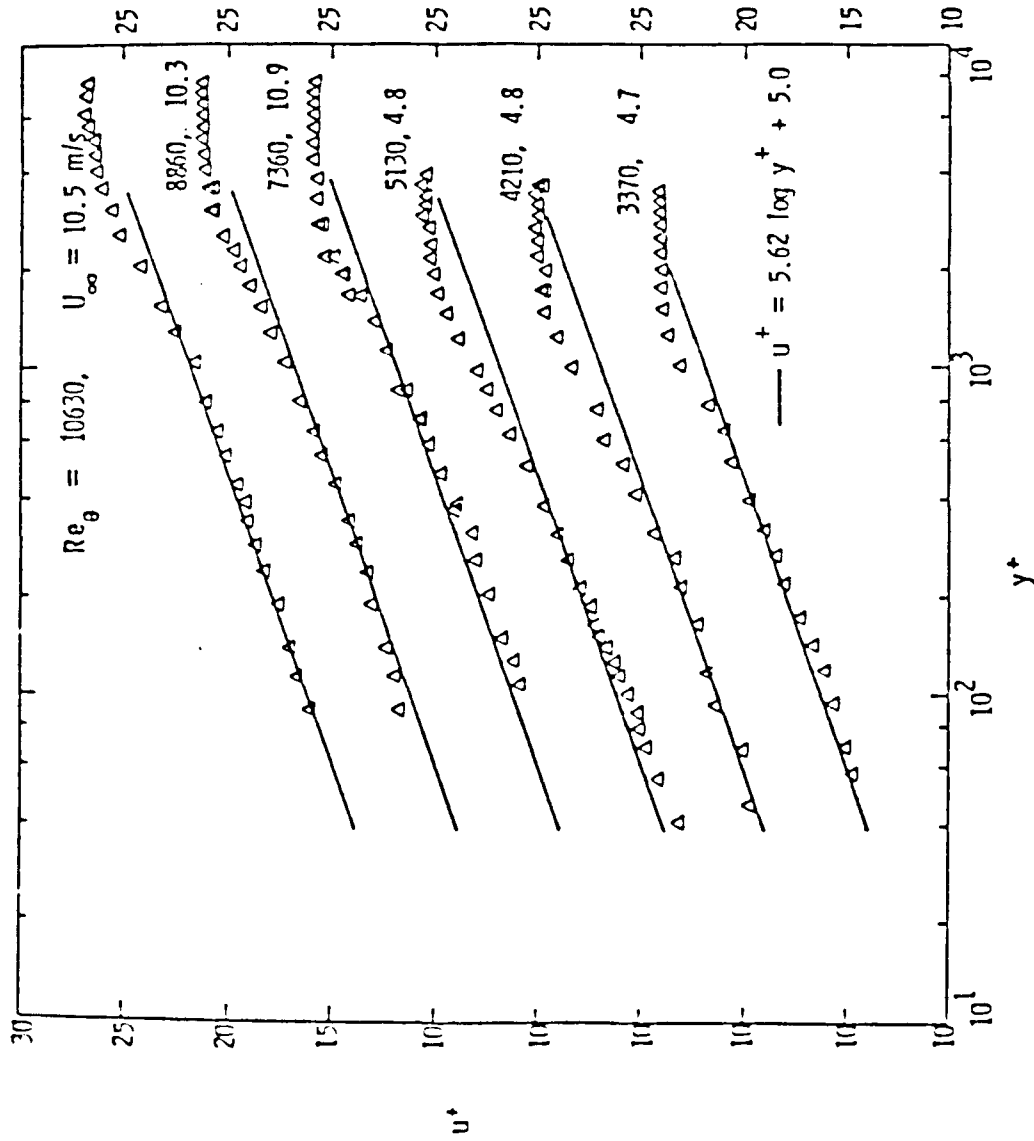stations.

Figure 3.   LDA velocity profile measurements in the undisturbed boundary
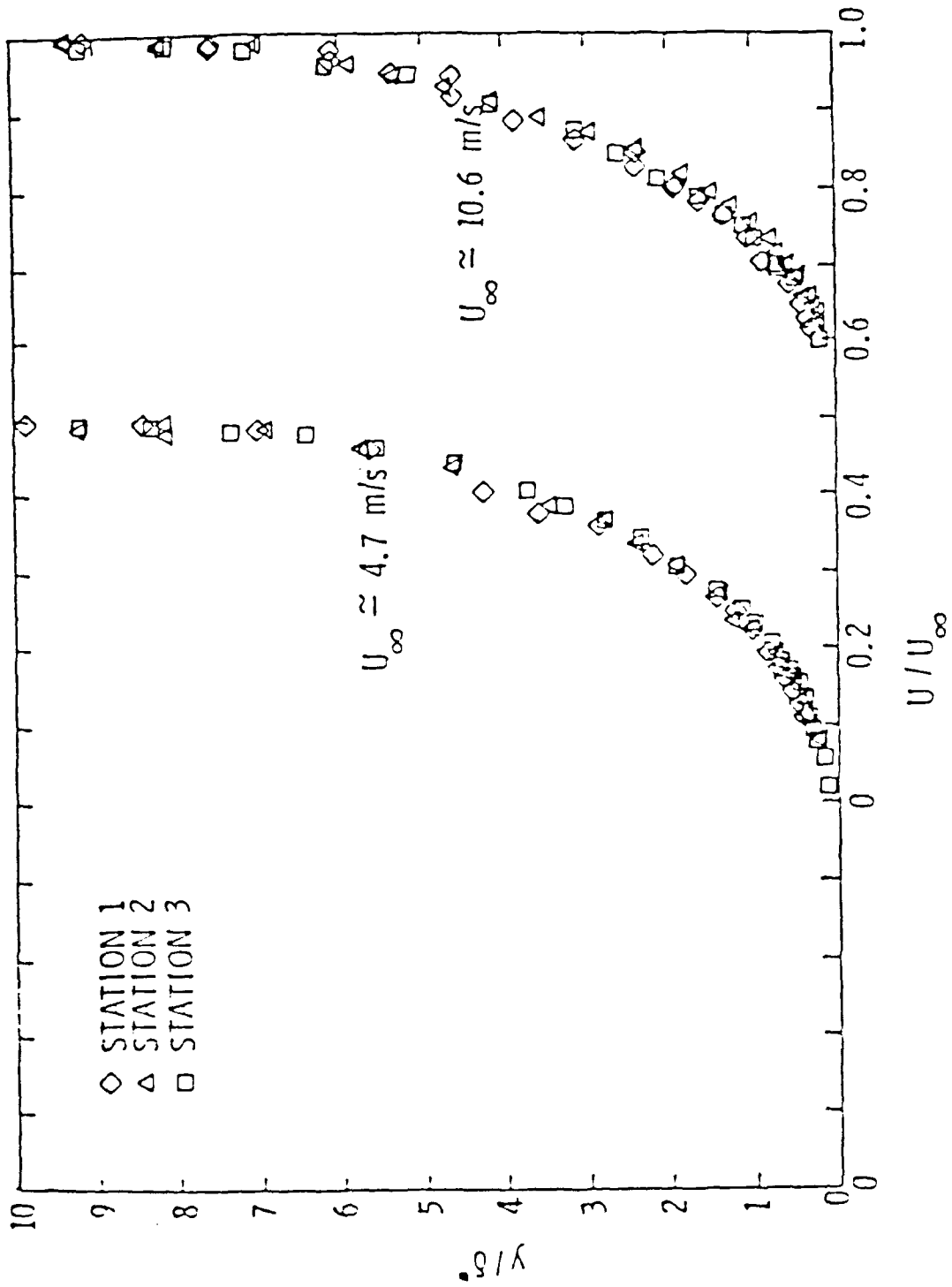layer presented in inner variables [Note shifted origins].

Figure 4.   LDA velocity profile measurements in the undisturbed boundary
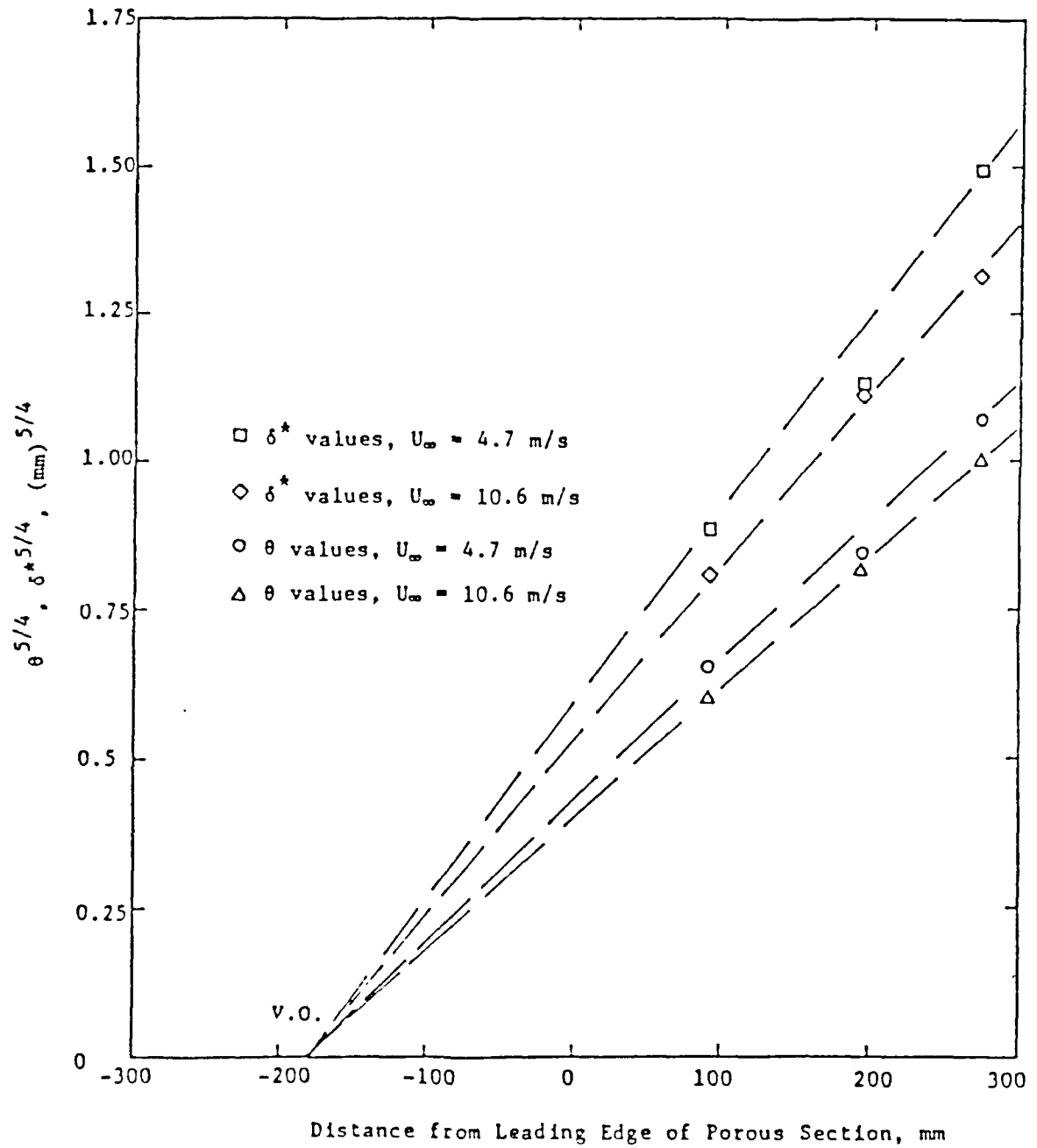layer presented in outer variables [Note shifted origins].

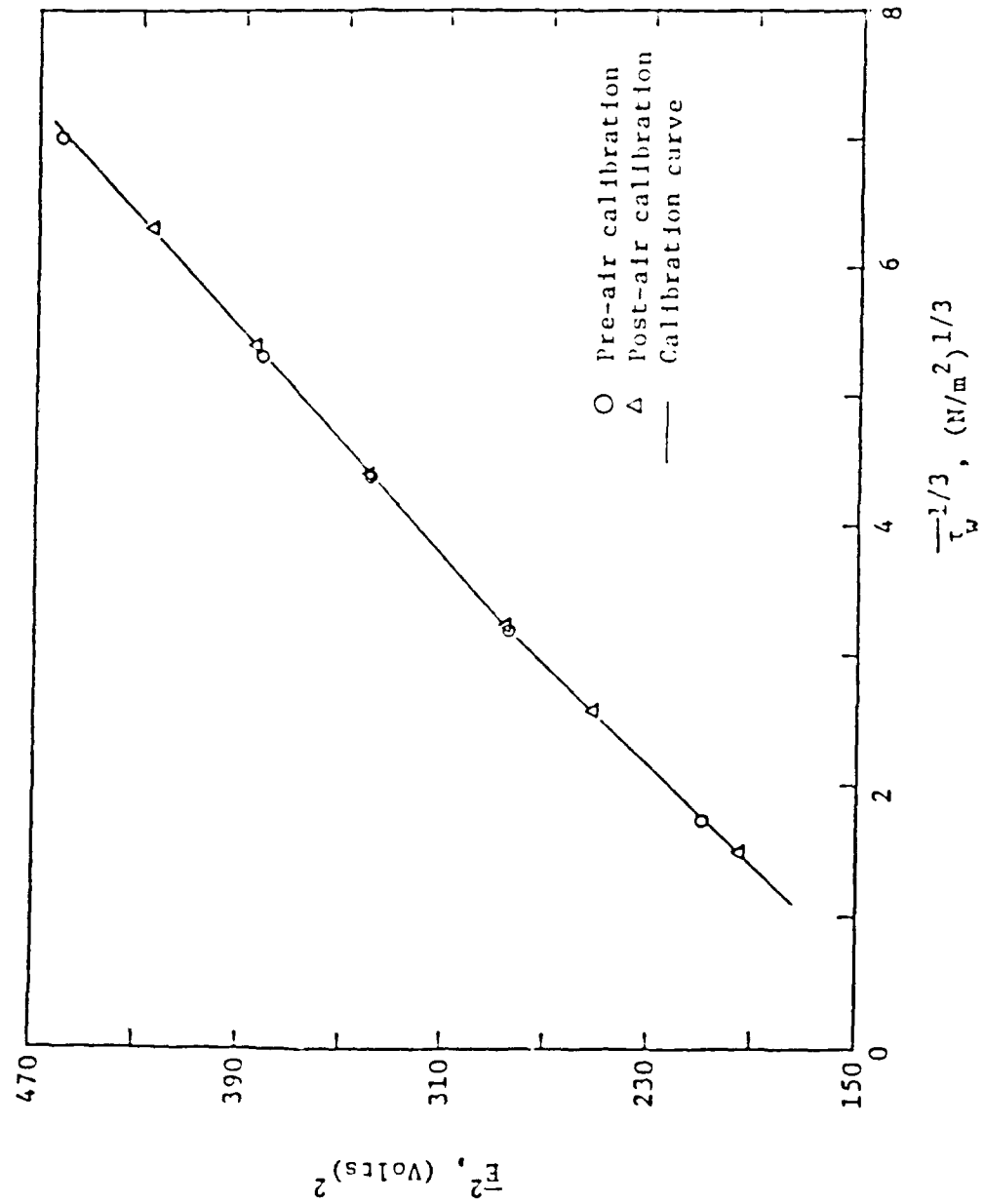Figure 5.   Determination of the virtual origin.

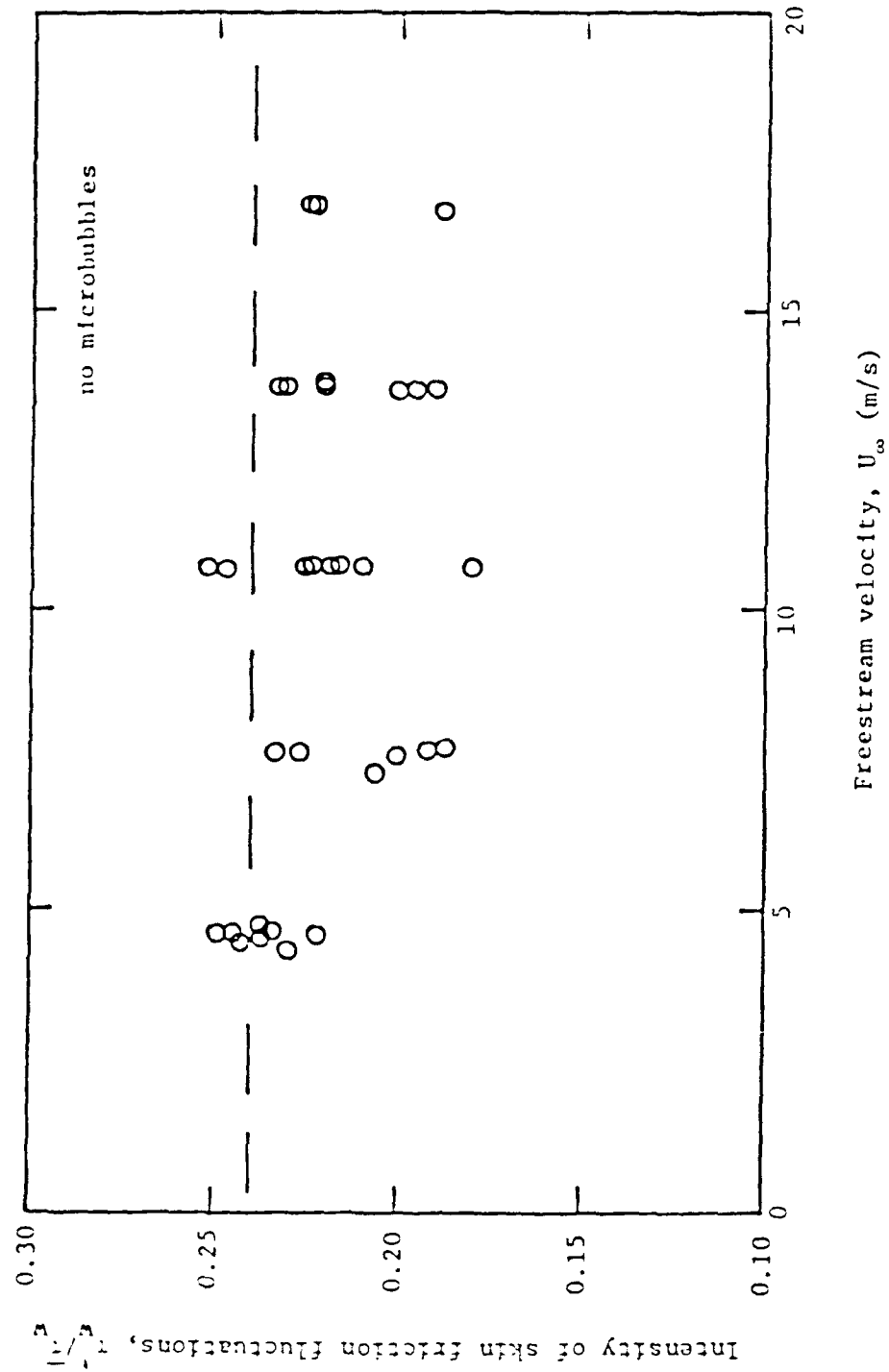Figure 6.   A typical calibration curve for the flush-mounted hot film
probes.

Figure 7.   Hot-film measurements of the skin friction fluctuations in the
undisturbed boundary layer. The Reynolds number is based on
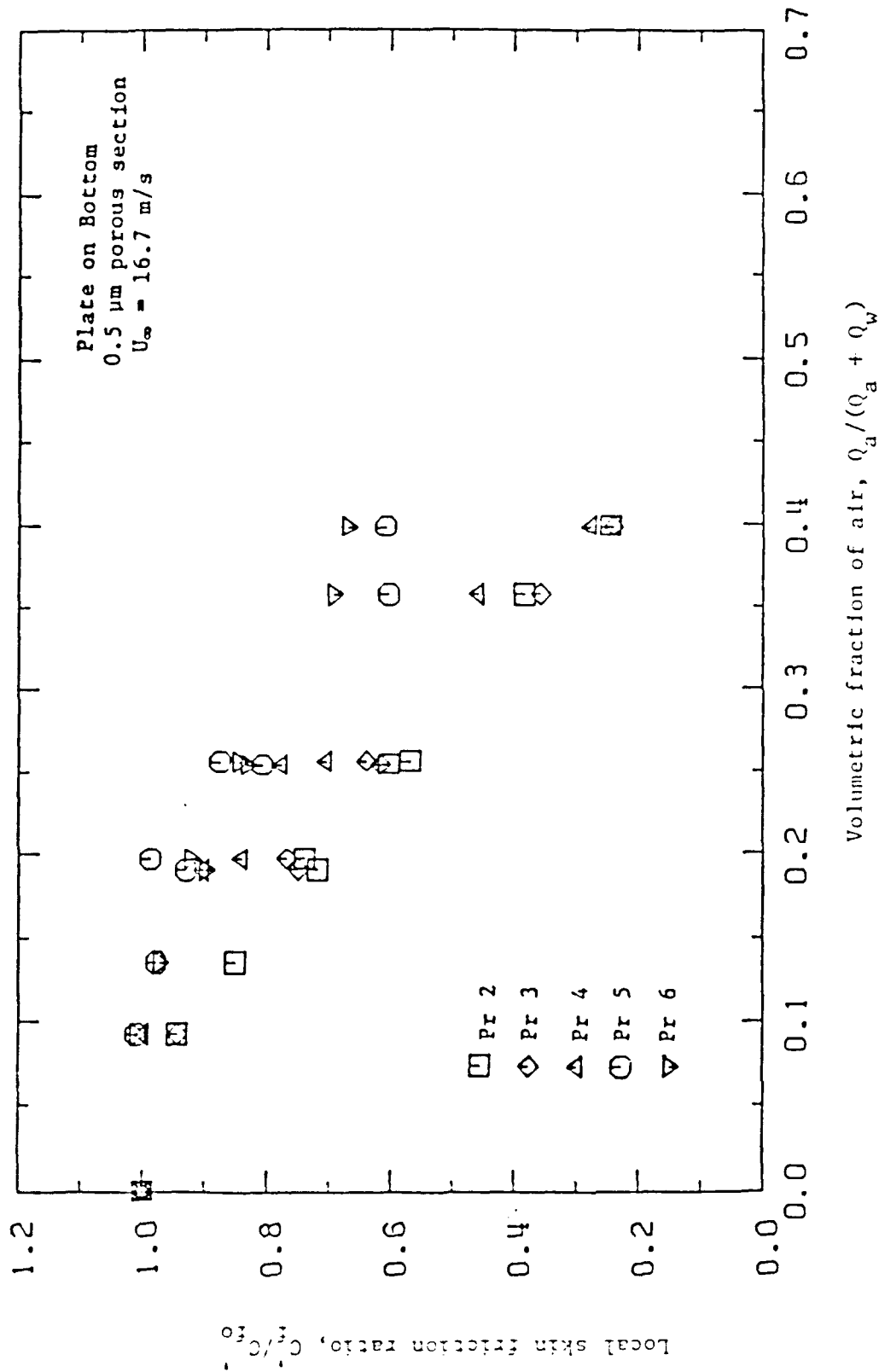the distance of the respective probe from the virtual origin.

Figure 8.   Hot-film measurements of the local skin friction with micro-
bubbles as a function of the air flow rate when the plate is
below the boundary layer. U_∞ = 16.7 m/s.

Figure 9.   Hot-film measurements of the local skin friction with micro-
bubbles as a function of the air flow rate when the plate is
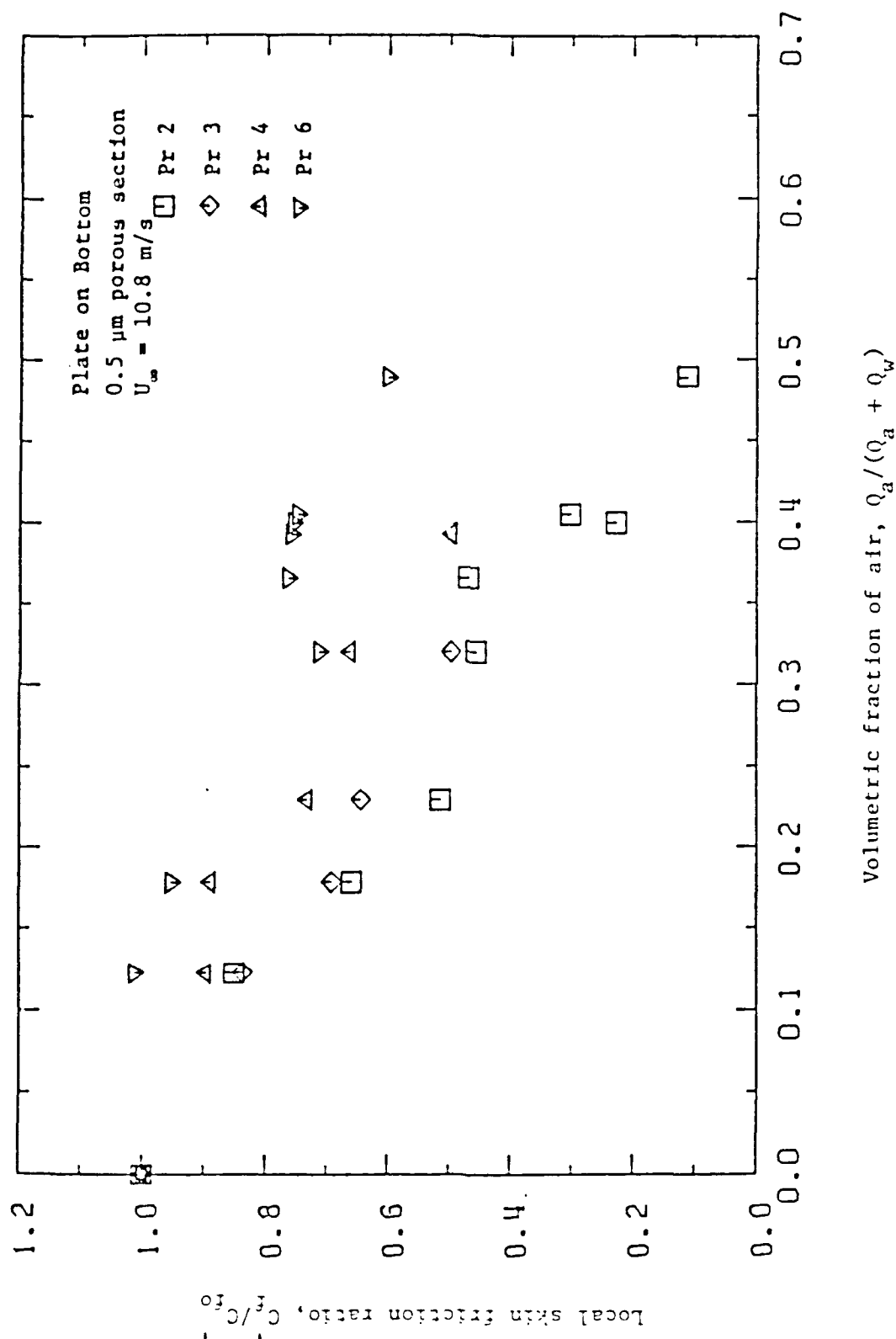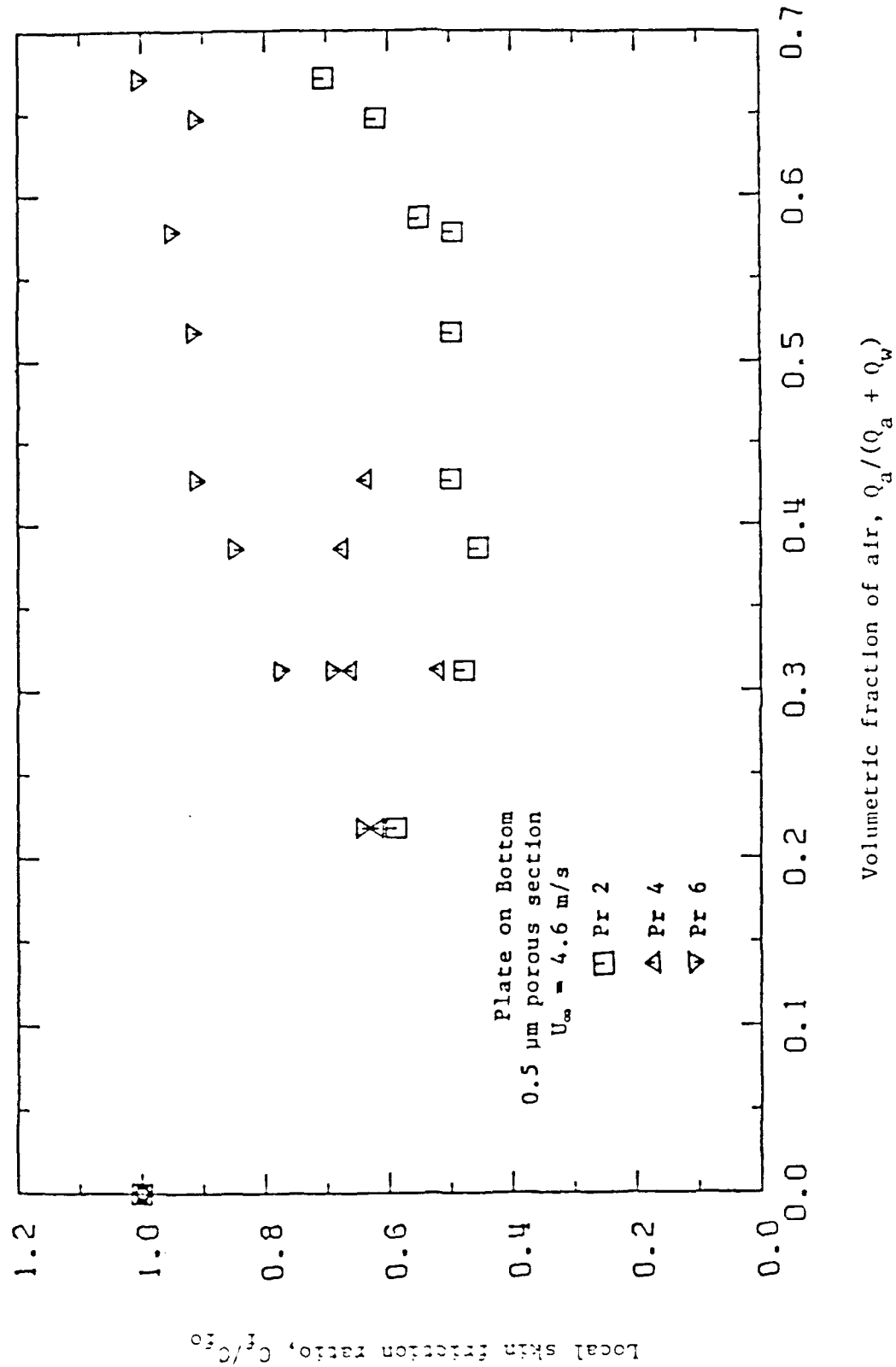below the boundary layer. U_∞ = 10.8 m/s.

Figure 10.   Hot-film measurements of the local skin friction with micro-
bubbles as a function of the air flow rate when the plate is
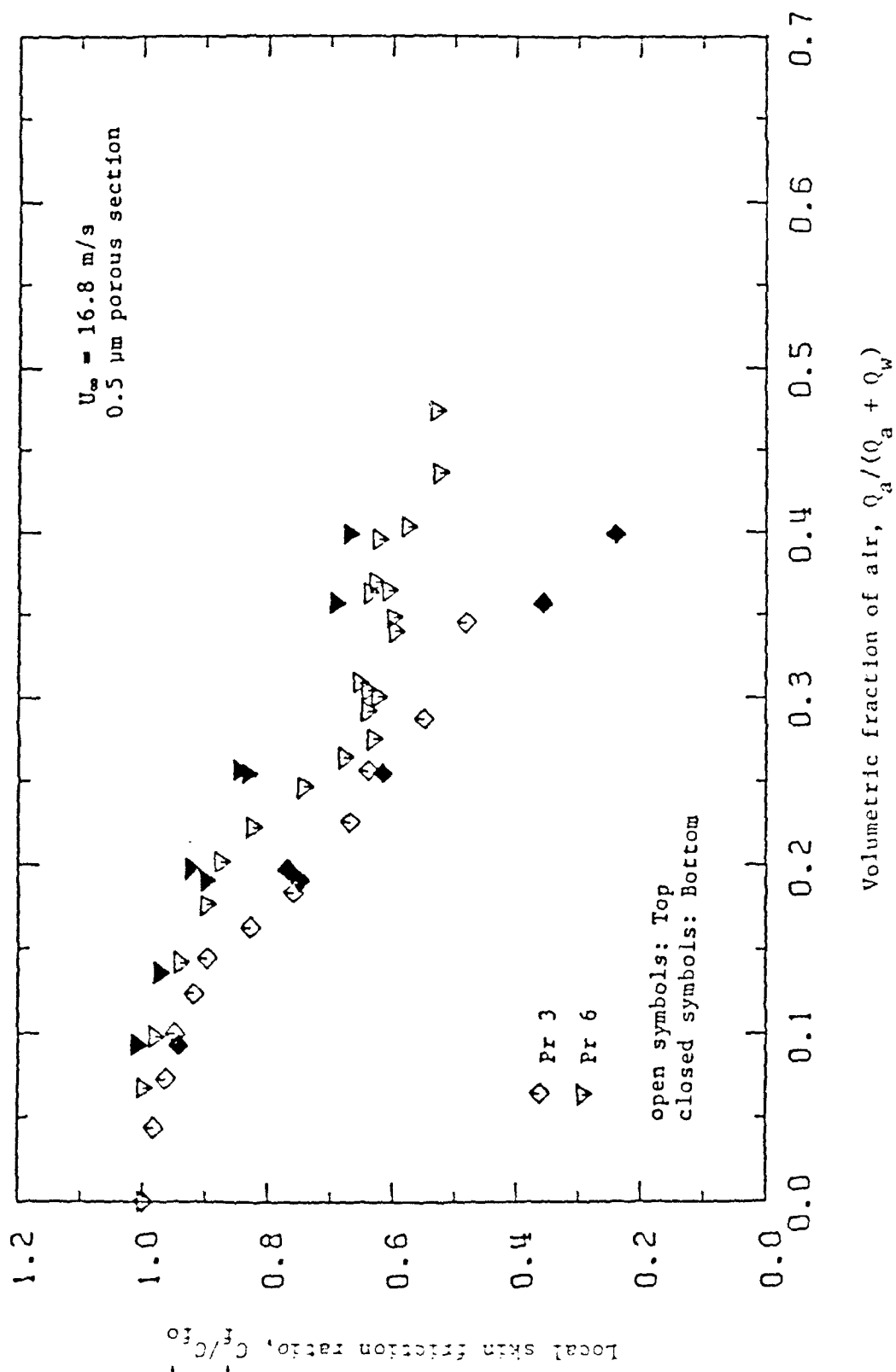below the boundary layer. U_∞ = 4.6 m/s.

Figure 1. Schematic of an experimental setup.

Pr - denotes flush-mounted hot film probe location
LDA - denotes LDA measurement station

	Distance to virtual origin, mm	Distance to leading edge of porous section, mm
Pr 1	170	-10
Pr 2	409	229
Pr 3	460	280
Pr 4	511	331
Pr 5	555	375
Pr 6	575	395
LDA 1	272	92
LDA 2	374	194
LDA 3	454	274

Figure 2. Schematic showing hot film probe locations and LDA measurement stations.

Figure 3. LDA velocity profile measurements in the undisturbed boundary layer presented in inner variables [Note shifted origins].

Figure 4. LDA velocity profile measurements in the undisturbed boundary layer presented in outer variables [Note shifted origins].

Figure 5. Determination of the virtual origin.

Figure 6. A typical calibration curve for the flush-mounted hot film probes.

Figure 7. Hot-film measurements of the skin friction fluctuations in the undisturbed boundary layer. The Reynolds number is based on the distance of the respective probe from the virtual origin.

Figure 8. Hot-film measurements of the local skin friction with
microbubbles as a function of the air flow rate when
the plate is below the boundary layer. $U_\infty = 16.7$ m/s.

Figure 9. Hot-film measurements of the local skin friction with microbubbles as a function of the air flow rate when the plate is below the boundary layer. $U_\infty = 10.8$ m/s.

Figure 10. Hot-film measurements of the local skin friction with microbubbles as a function of the air flow rate when the plate is below the boundary layer. $U_\infty = 4.6$ m/s.

Figure 11. The effect of gravity on the hot-film measurements
of the local skin friction with microbubbles.
Comparison of data taken with the plate above and
below the boundary layer. $U_\infty = 16.8$ m/s.
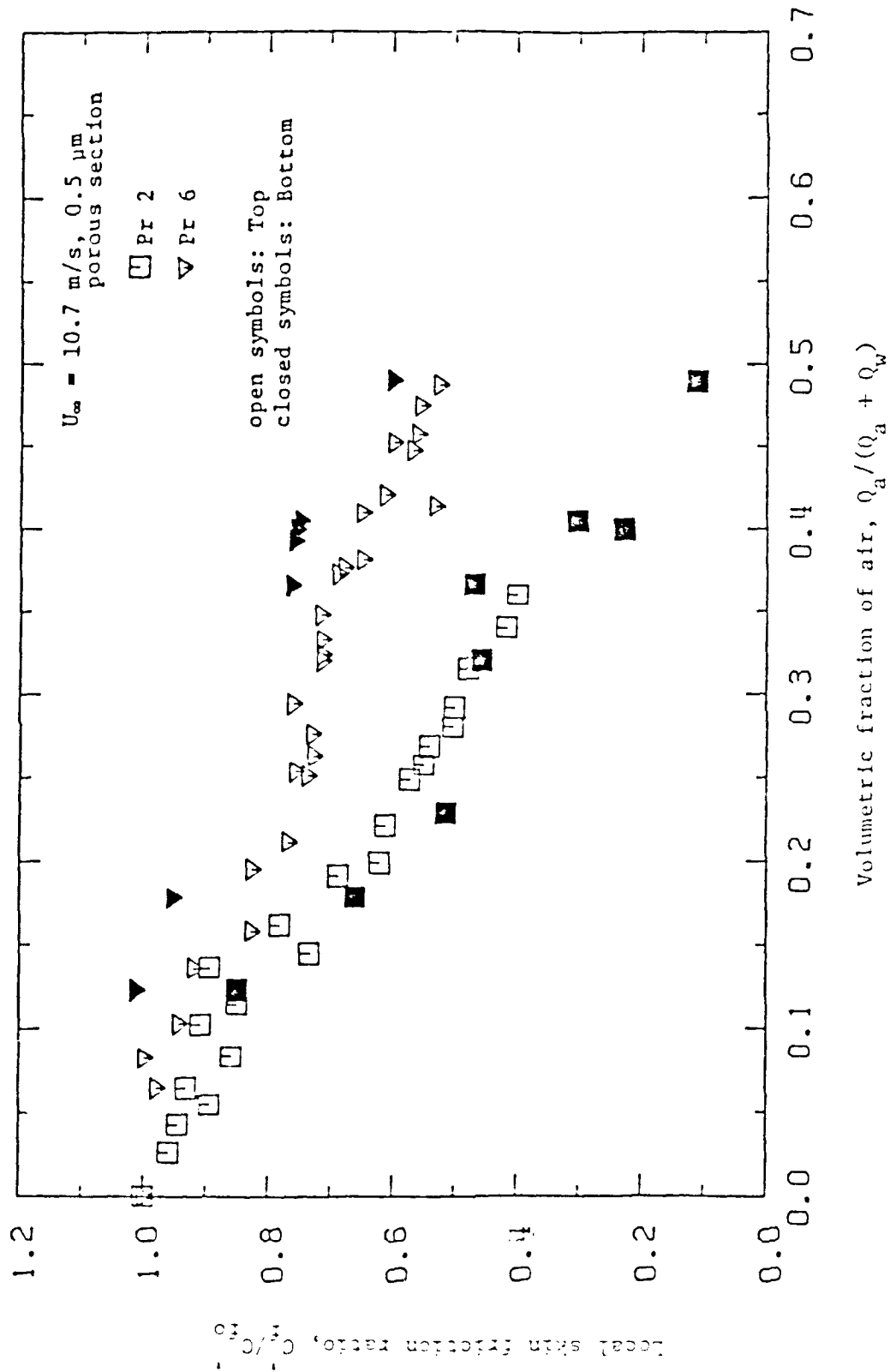
Figure 12. The effect of gravity on the hot-film measurements of the local skin friction with microbubbles. Comparison of data taken with the plate above and below the boundary layer. $U_\infty = 10.7$ m/s.
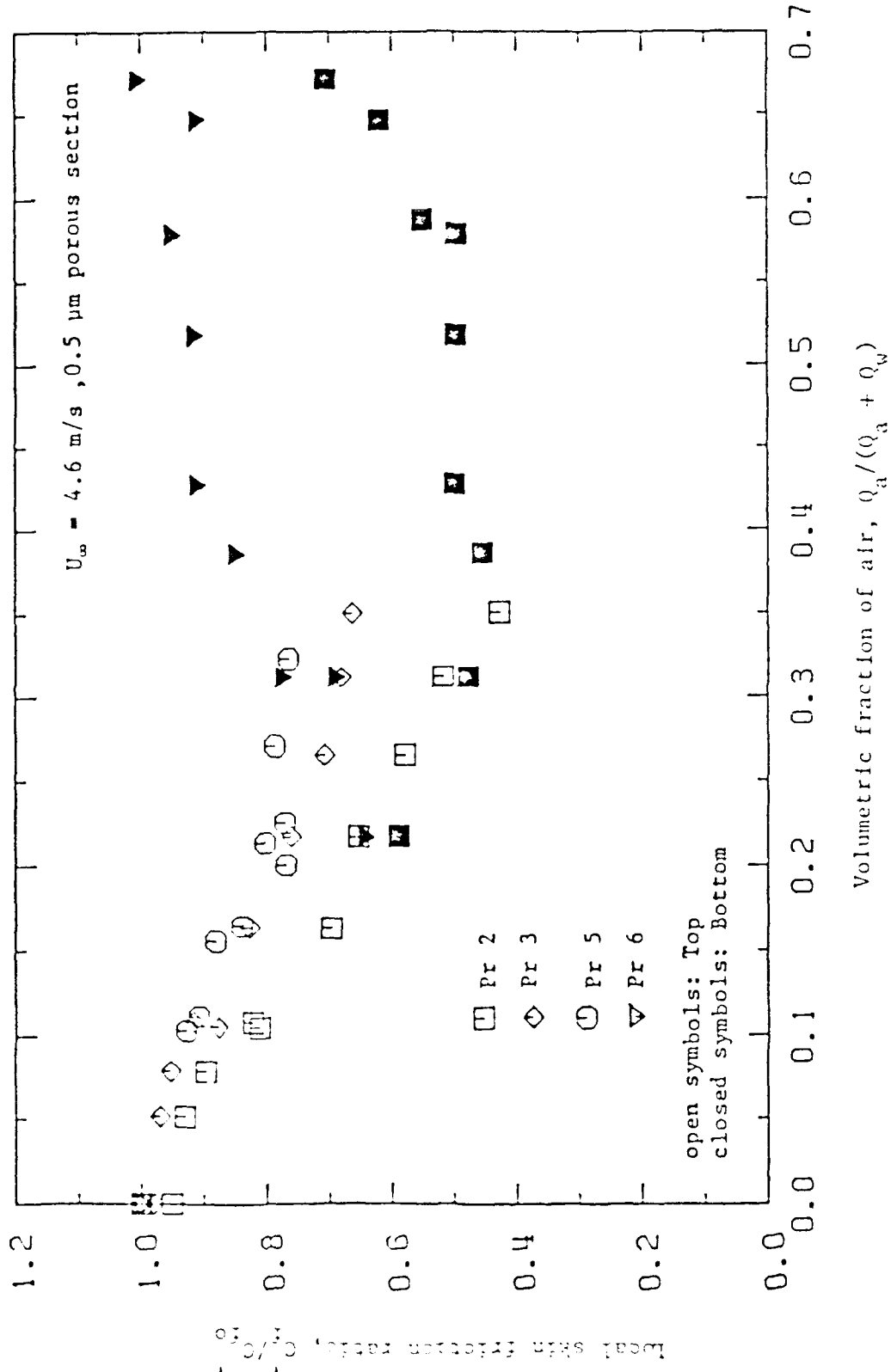
Figure 13. The effect of gravity on the hot-film measurements of the local skin friction with microbubbles. Comparison of data taken with the plate above and below the boundary layer. $U_\infty = 4.6$ m/s.
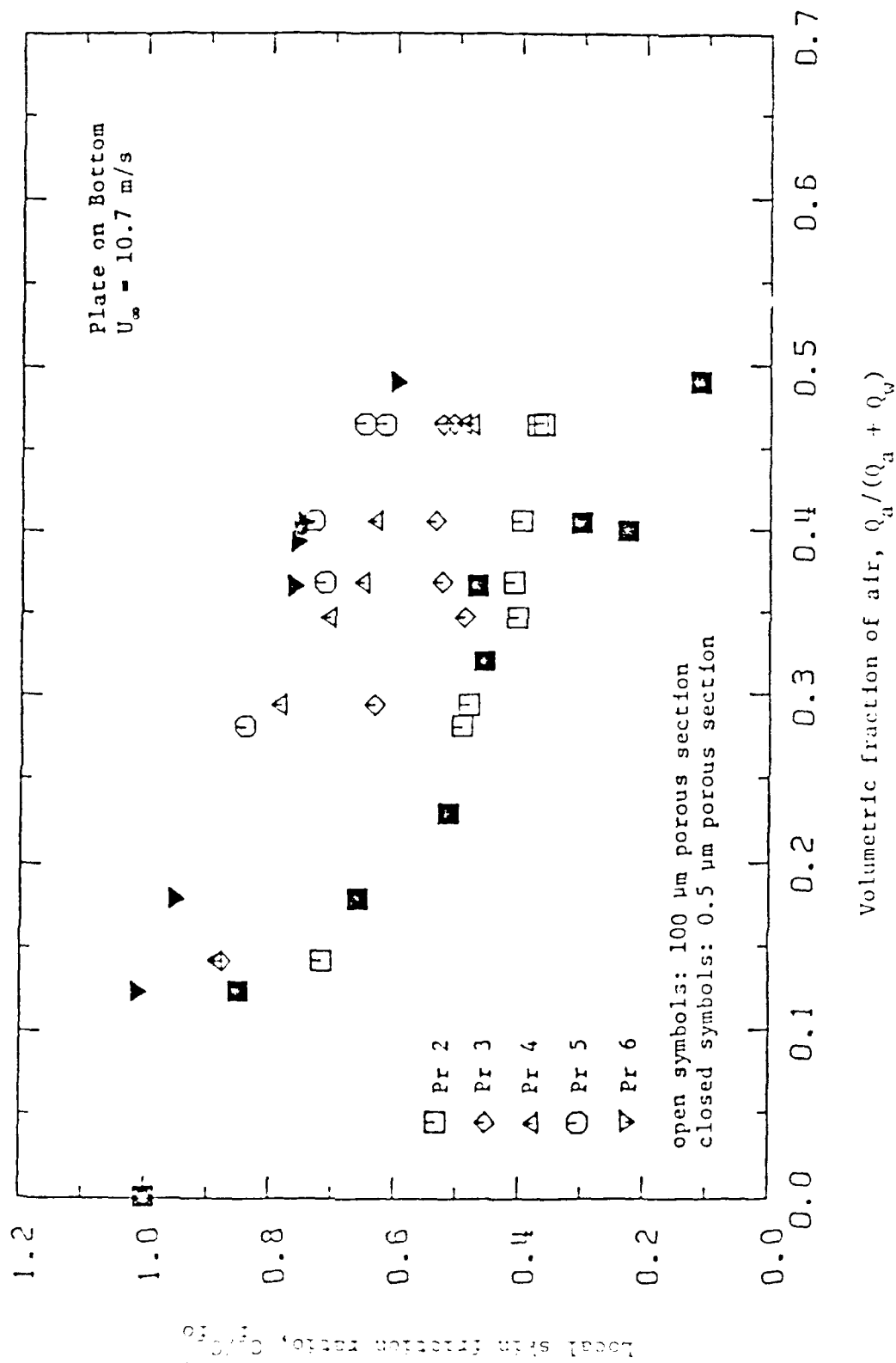
Figure 14. The effect of pore size variations on the local skin friction measurements. Comparison of data taken with the 0.5 μm and 100 μm porous sections. U_∞ = 16.8 m/s.
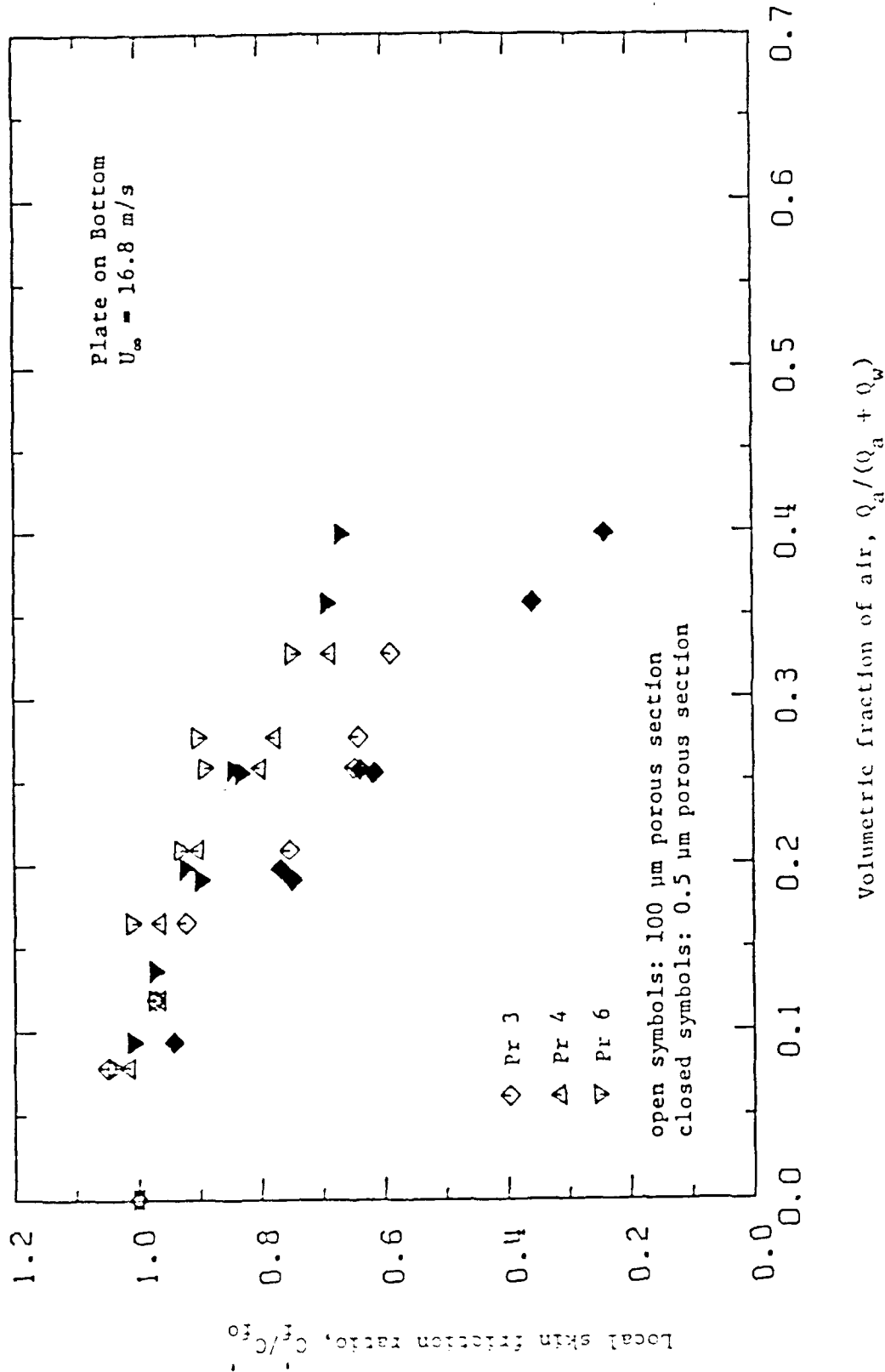
Figure 15. The effect of pore size variations on the local skin friction measurements. Comparison of data taken with the 0.5 μm and 100 μm porous sections. $U_\infty = 10.7$ m/s.
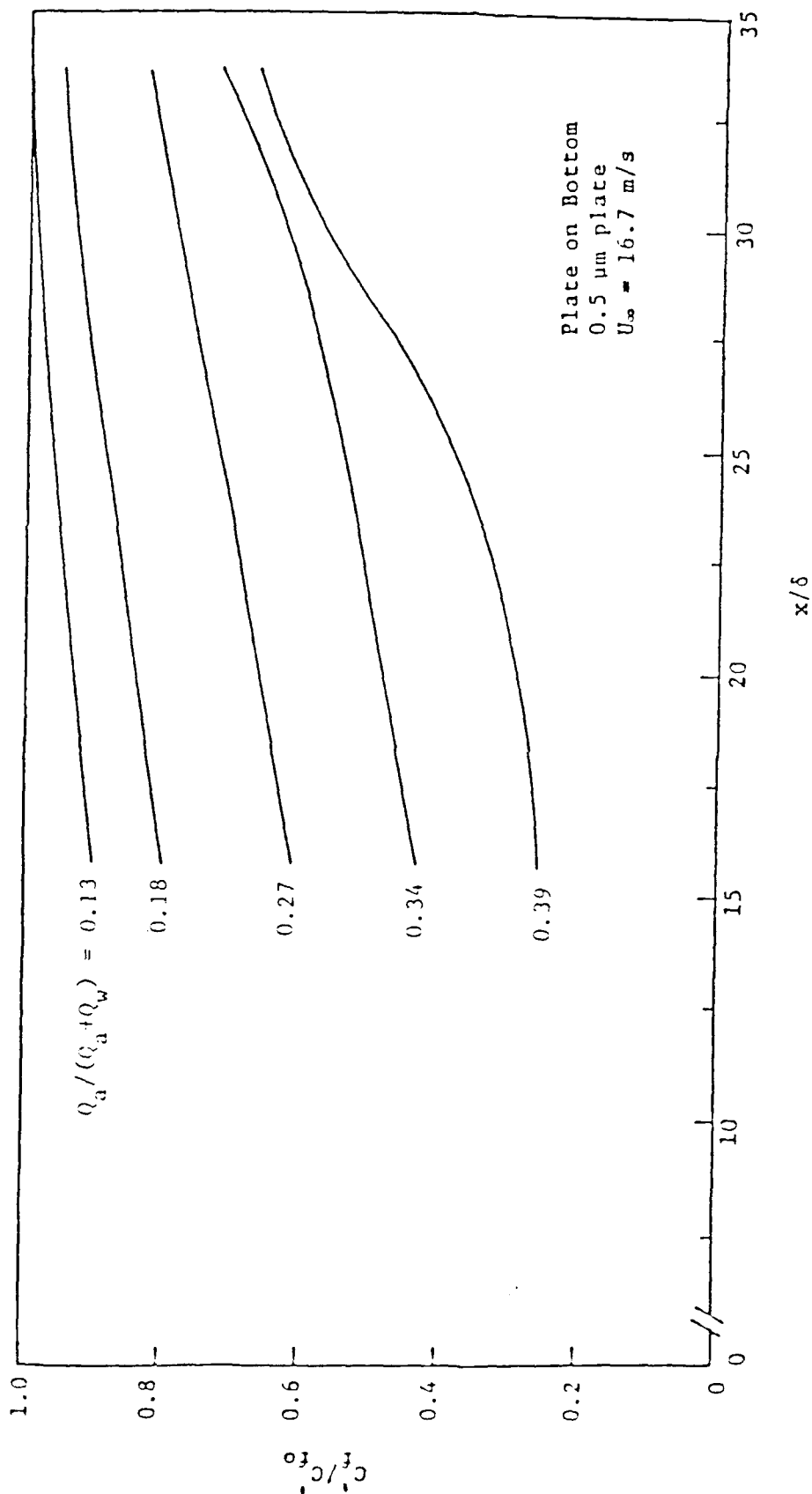
Figure 16. The downstream persistence of the skin friction reduction. The plate is below the boundary layer. $(U_\infty = 16.7 \text{ m/s})$.
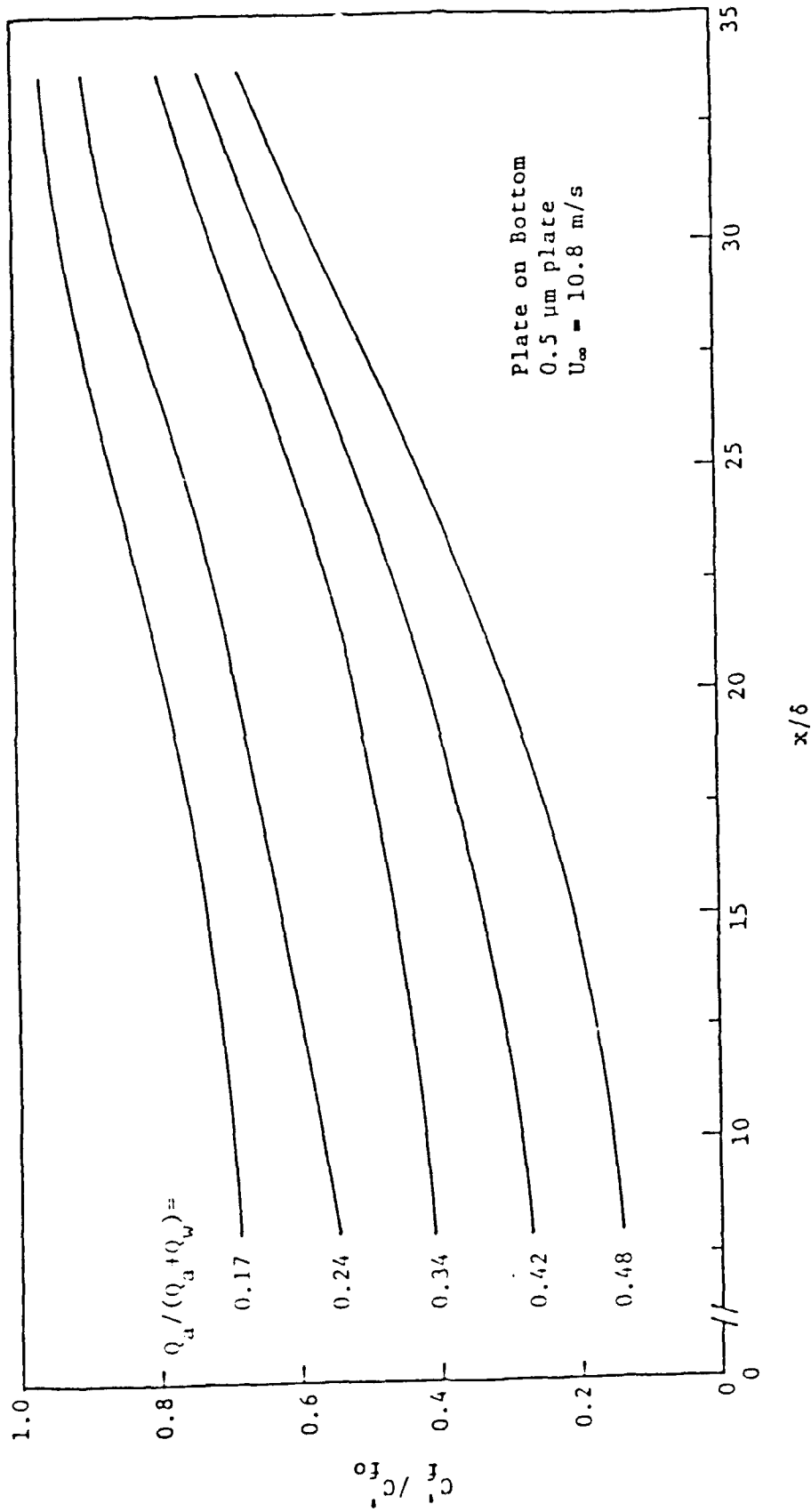
Figure 17. The downstream persistence of the skin friction reduction. The plate is below the boundary layer. $U_\infty = 10.8$ m/s.
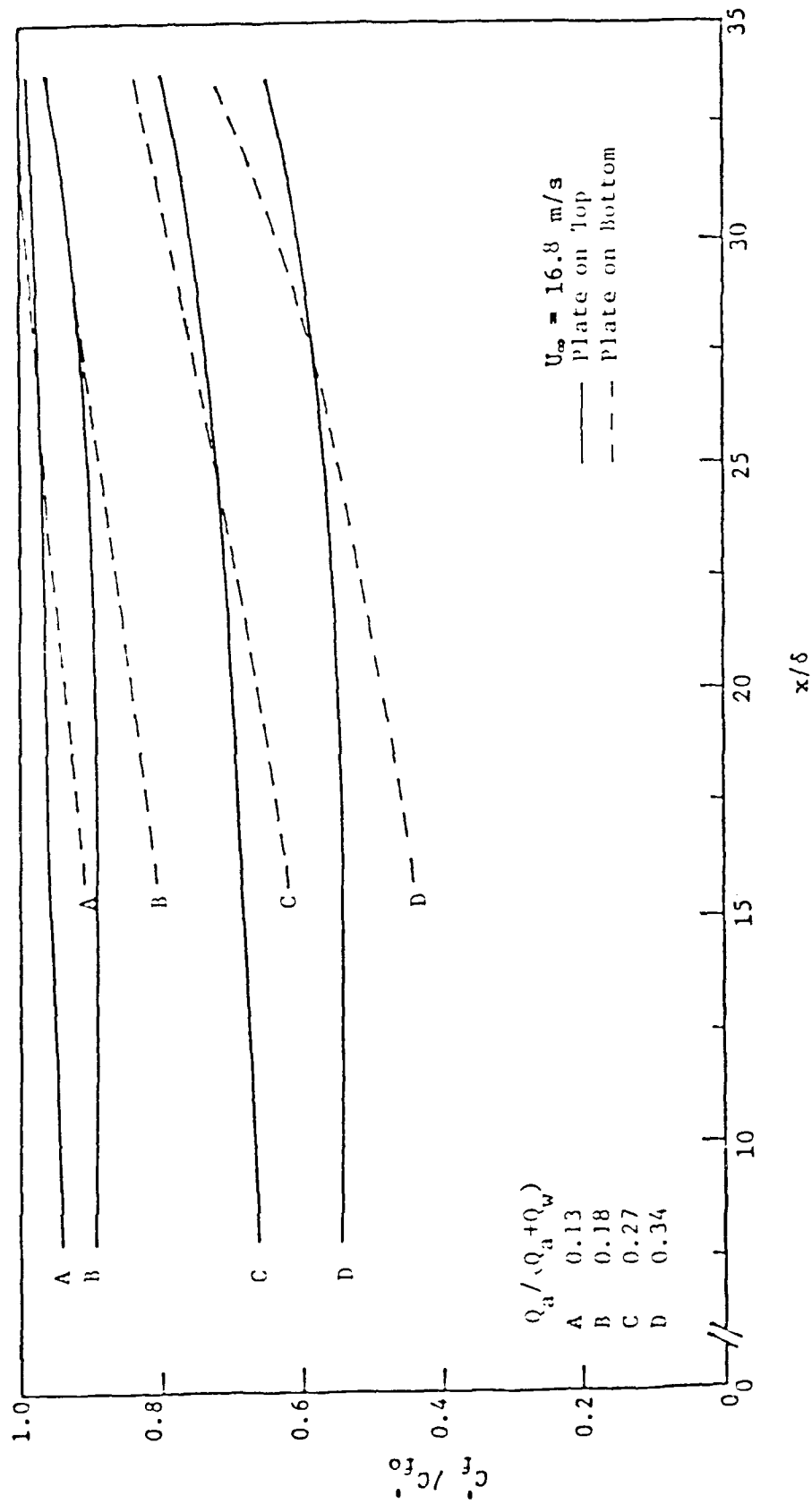
Figure 18. The downstream persistence of the skin friction reduction. Comparison of data taken with the plate above and below the boundary layer. $U_\infty = 16.8$ m/s.
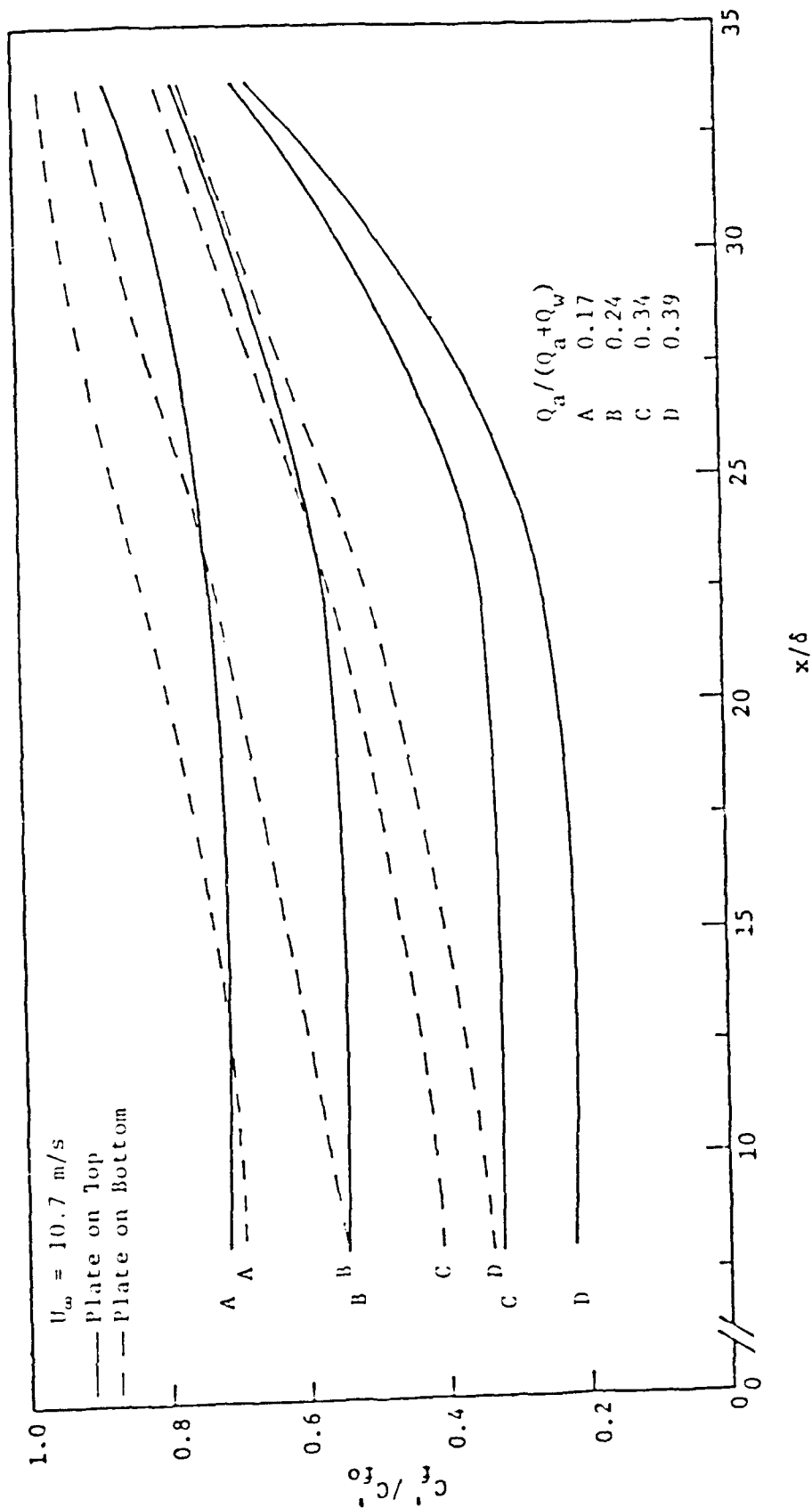
Figure 19.   The downstream persistence of the skin friction
             reduction.   Comparison of data taken with the
             plate above and below the boundary layer.
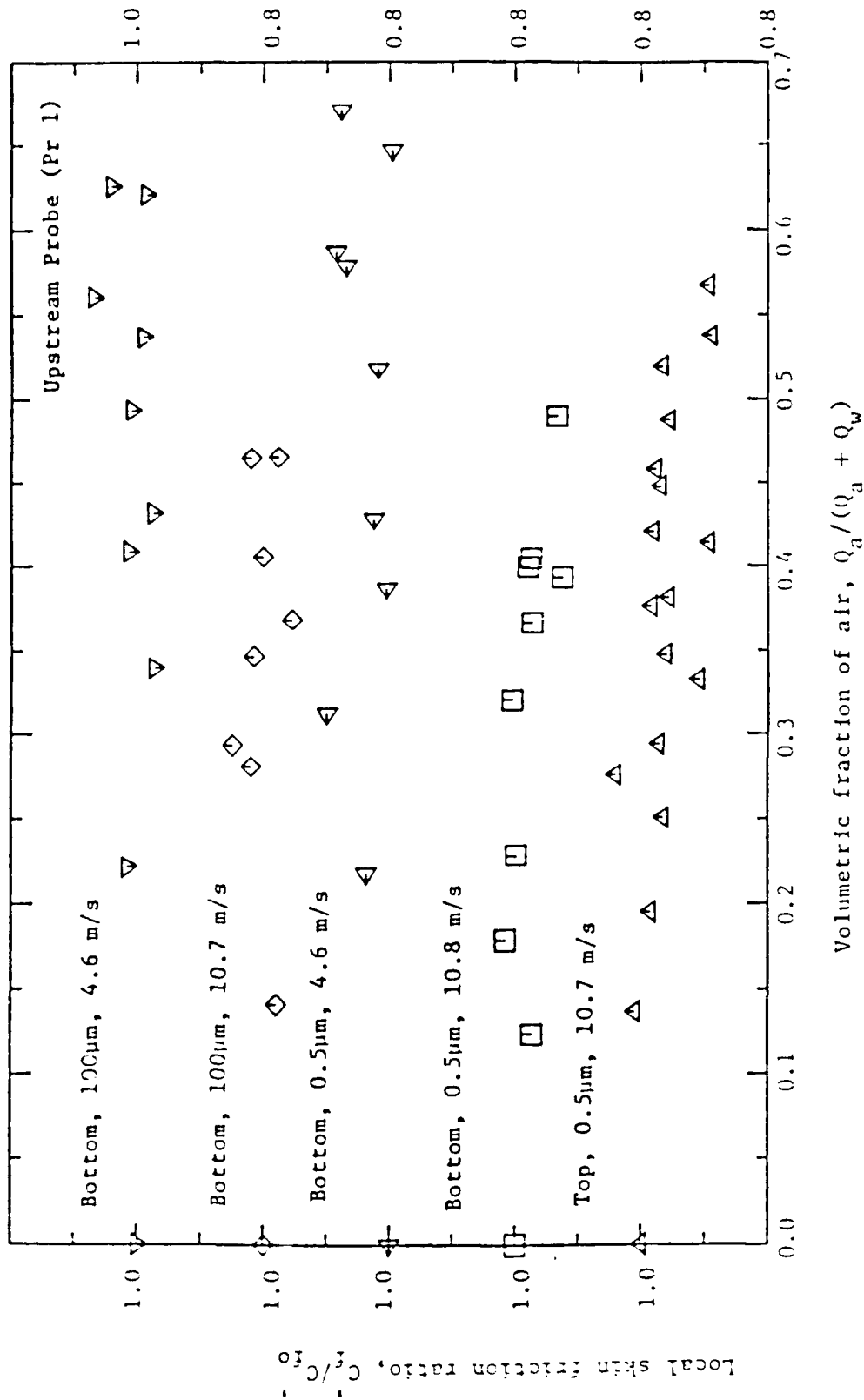 $U_\infty = 10.7$ m/s.

Figure 20. Hot-film measurements of the local skin friction upstream of microbubble introduction into the boundary layer [Note shifted origins].
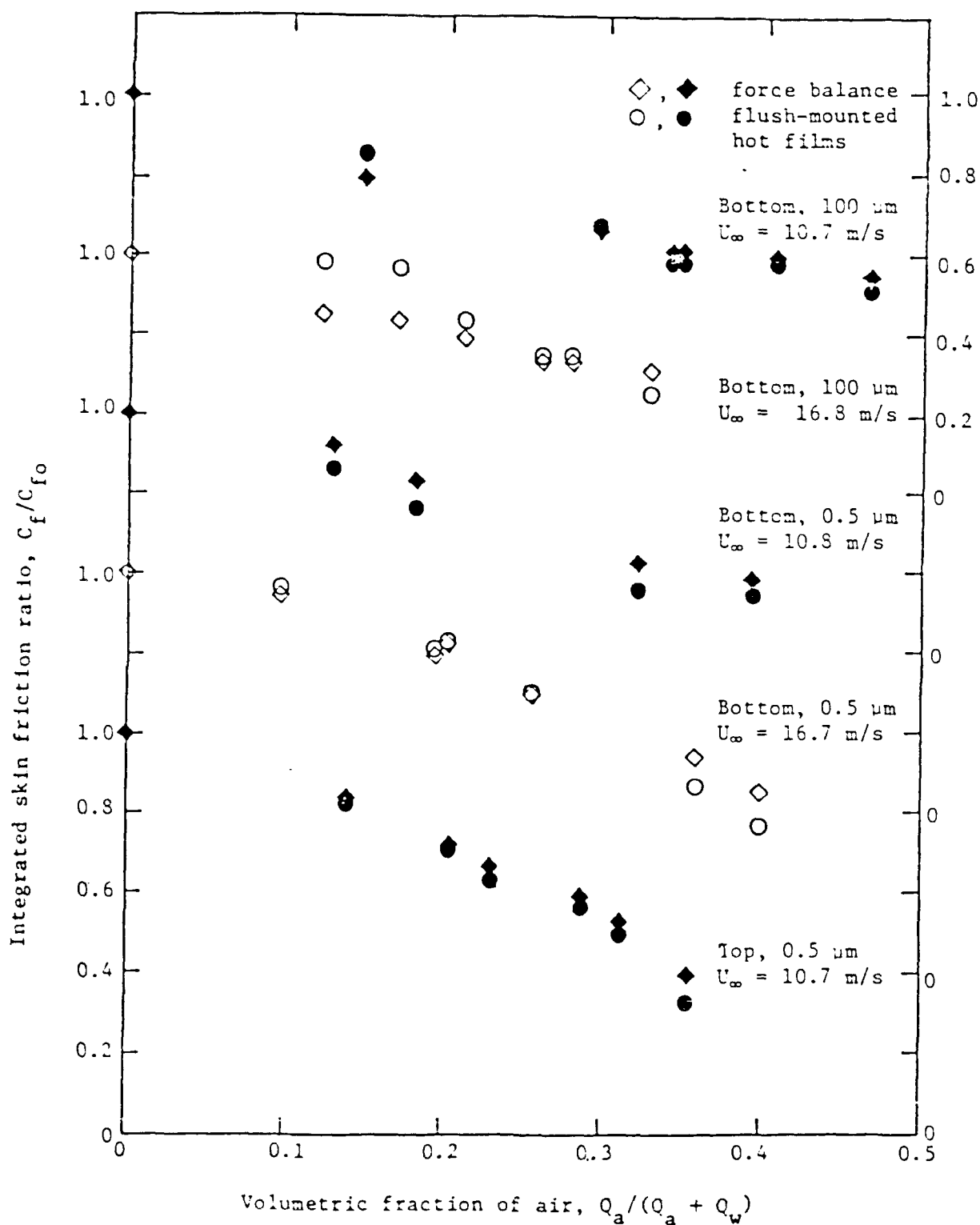
Figure 21.   Comparison of the integrated skin friction reductions
with microbubbles measured by the force balance with
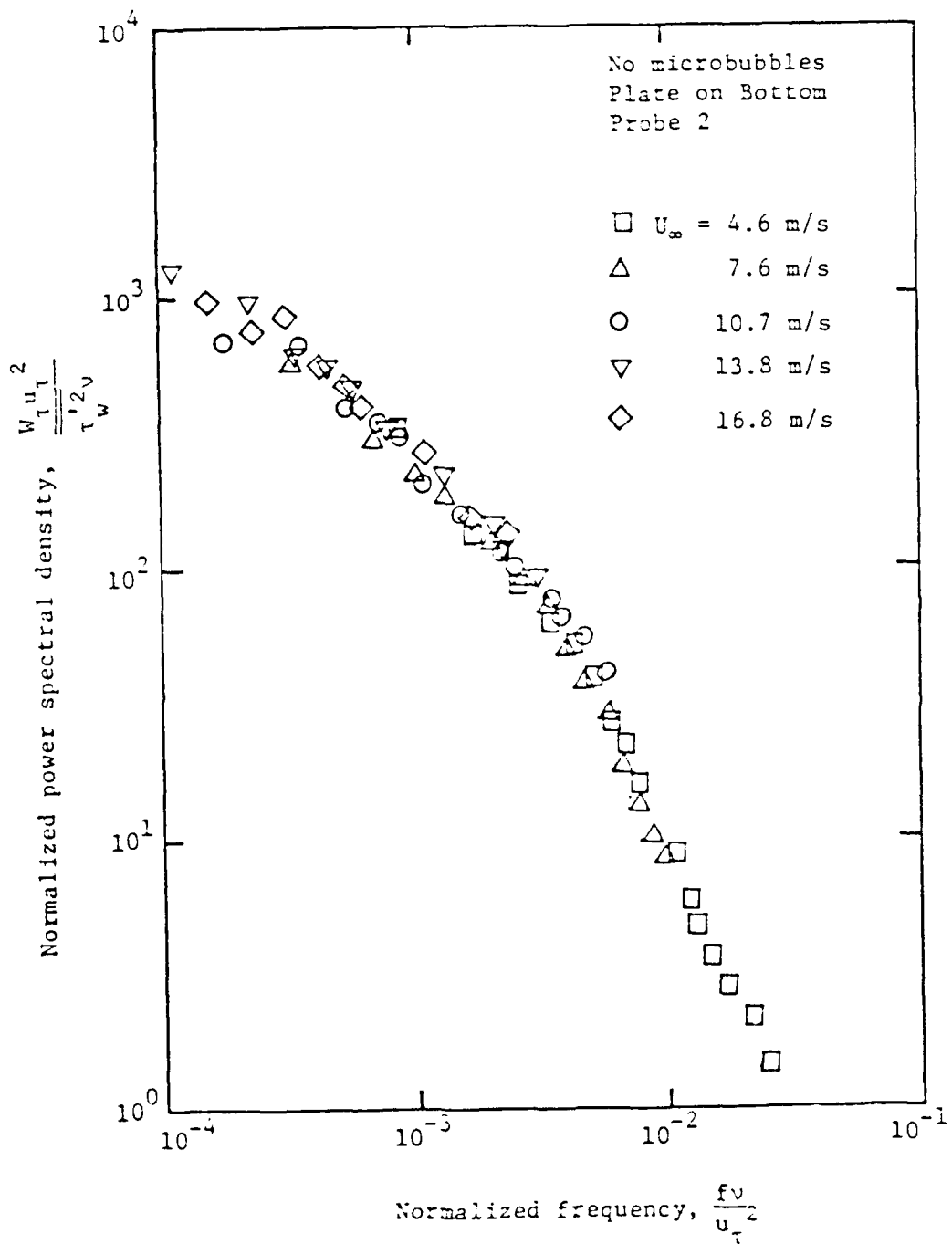that evaluated from the hot films.

Figure 22. Normalized power spectral density functions of the hot-film signals in the presence and absence of microbubbles.
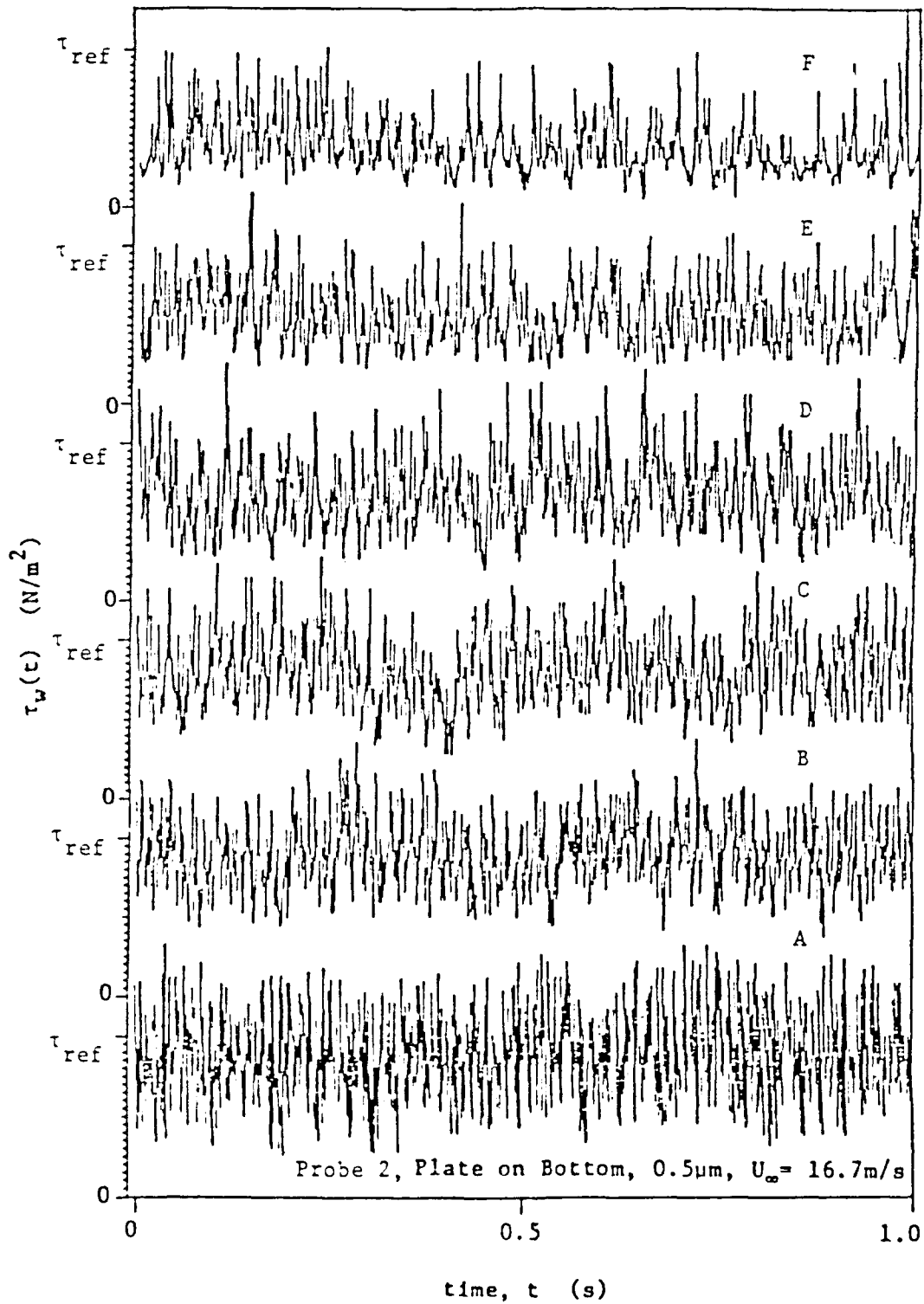
Figure 23. A sequence of linearized hot-film signal traces in
the presence and absence of microbubbles.
A: no microbubbles; B: 10% air, 5% C_f reduction;
C: 14% air, 15% C_f reduction; D: 19% air,
28% C_f reduction; E: 26% air, 40% C_f reduction;
and F: 36% air, 62% C_f reduction.

Figure 24.   Normalized power spectral density functions of the
             hot-film signal in the presence of microbubbles.
             (probe 2, plate on top, 10.7 m/sec).

Plate on Top
U_∞ = 10.7 m/s
Probe 2

$Q_a/(Q_a+Q_w)$

——— 0 (no air)

☐   0.17

◯   0.17

△   0.24

▽   0.25

◇   0.27

▷   0.34

Normalized power spectral density, $\dfrac{W_1 u_\tau^2}{\tau_w^2 \nu}$

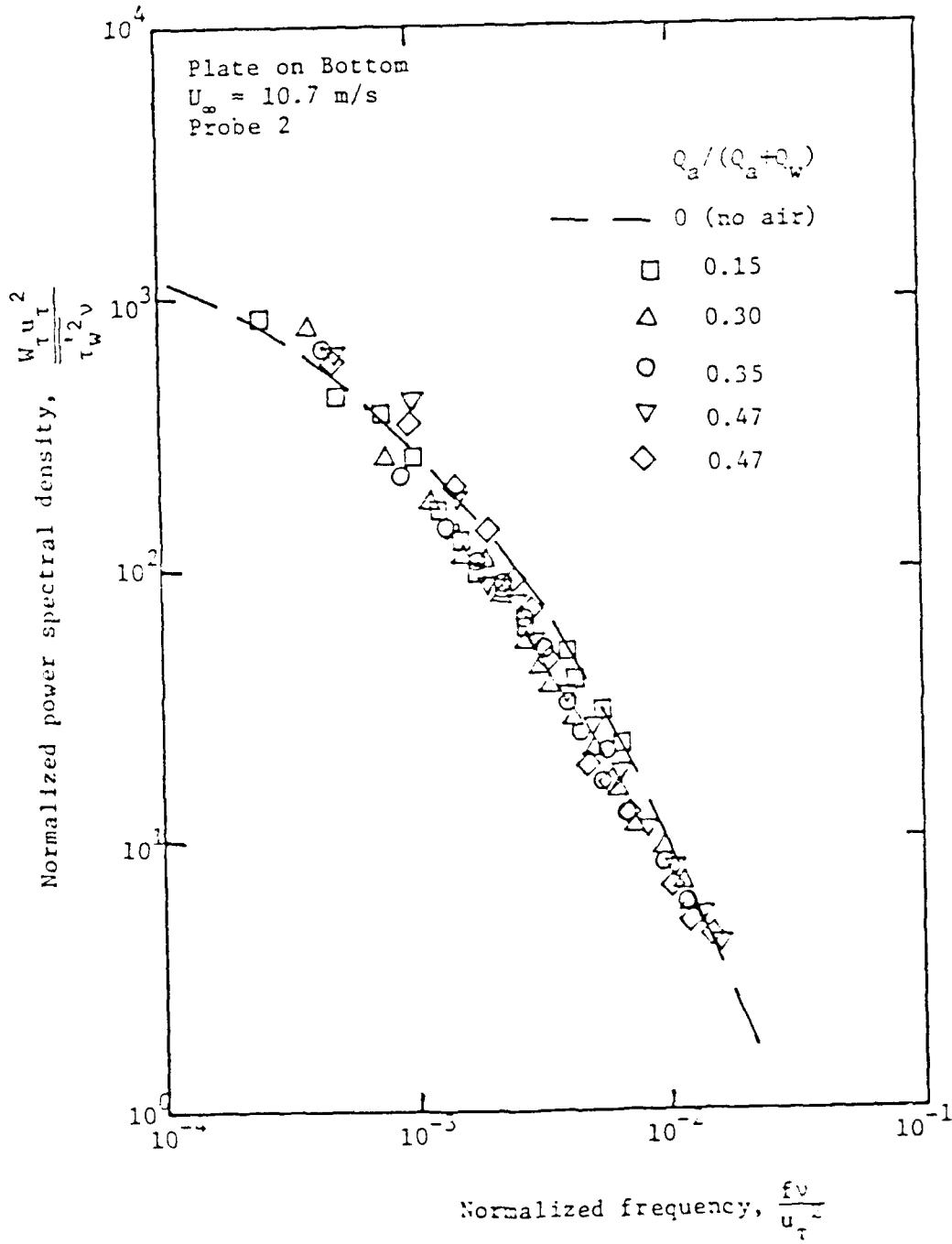Normalized frequency, $\dfrac{f\nu}{u_\tau^2}$
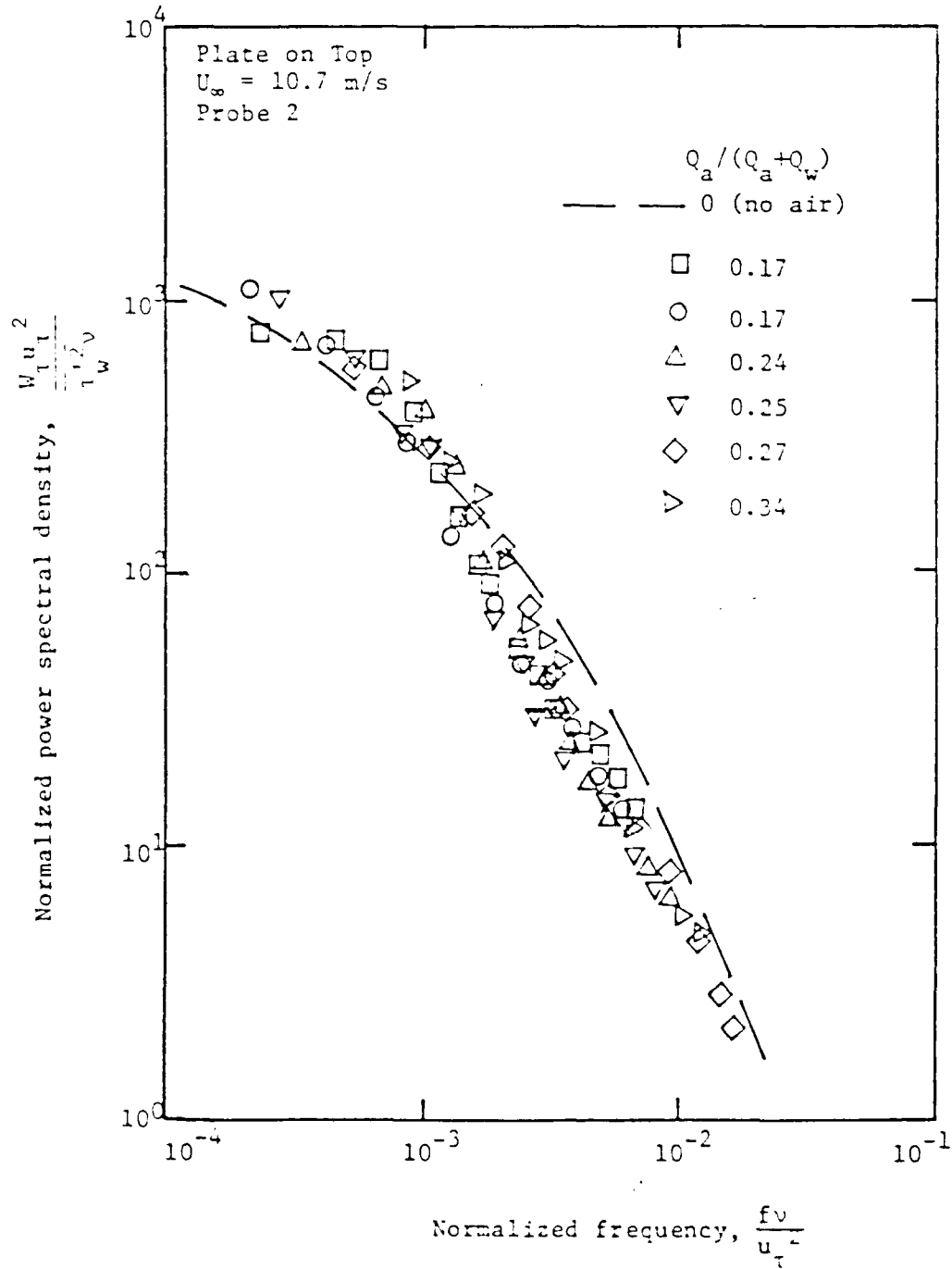
Figure 25. Normalized power spectral density functions of the
            hot-film signal in the presence of microbubbles.
            (probe 2, plate on bottom, 10.7 m/sec).
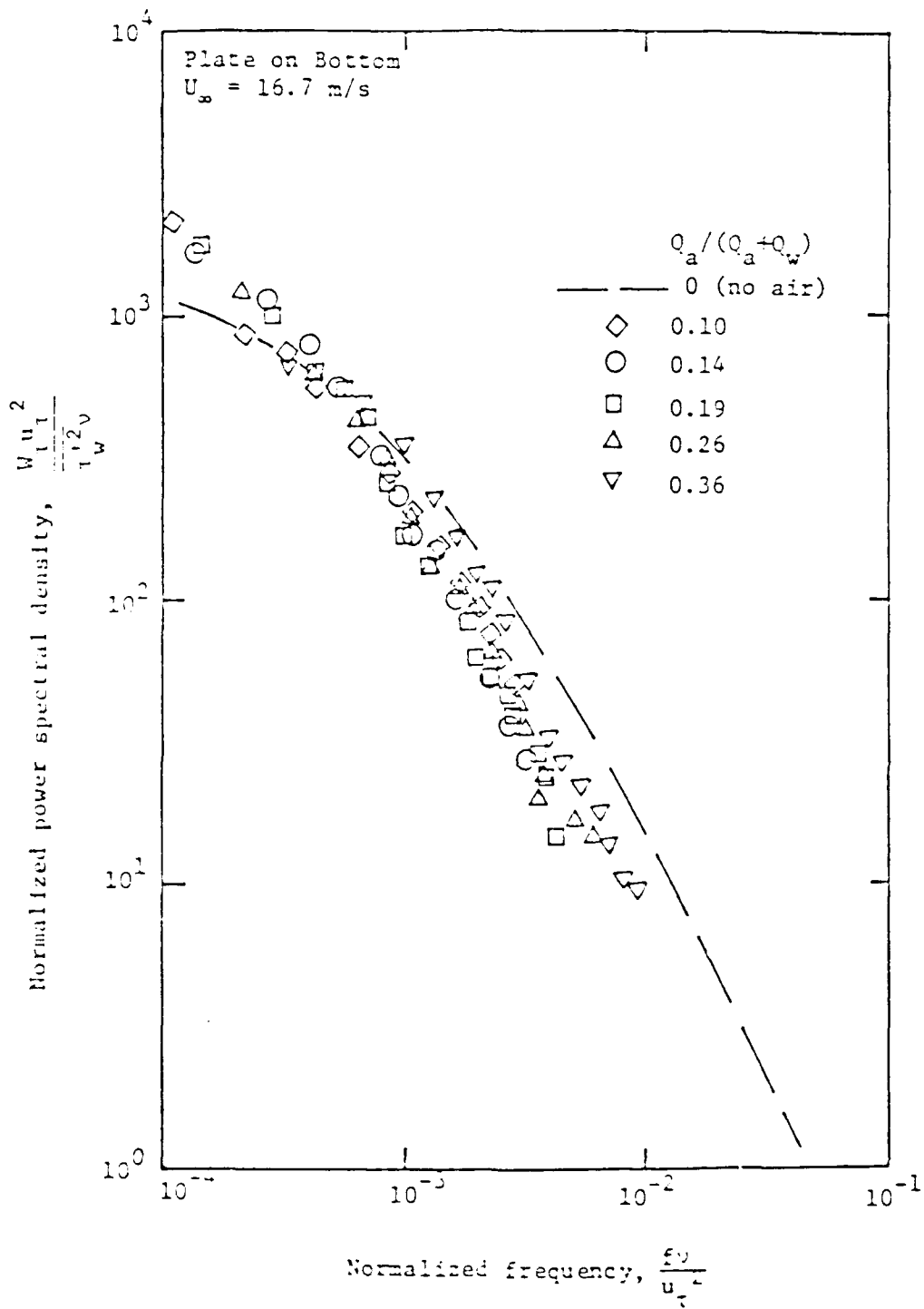
Figure 26. Normalized power spectral density functions of the
            hot-film signal in the presence of microbubbles.
            (probe 3, plate on bottom, 16.8 m/sec).

Distribution List for ARL/PSU Unclassified TM 84-136 by N. K. Madavan, S. Deutsch and C. L. Merkle, dated 24 August 1984

Commander
Naval Sea Systems Command
Department of the Navy
Washington, DC 20362
Attn: Library
        Code NSEA-09G32
(Copies 1 and 2)

Commanding Officer
Naval Underwater Systems Ctr.
Department of the Navy
Newport, RI 02840
Attn: Library
        Code 54
(Copy No. 8)

Commander
Naval Sea Systems Command
Department of the Navy
Washington, DC 20362
Attn: F. Romano
        Code NSEA-63R
(Copy No. 3)

Commanding Officer
Naval Underwater Systems Ctr.
Department of the Navy
Newport, RI 02840
Attn: T. A. Davis
        Code 36314
(Copy No. 9)

Commander
Naval Sea Systems Command
Department of the Navy
Washington, DC 20362
Attn: T. E. Peirce
        Code NSEA-63R31
(Copy No. 4)

Commanding Officer
Naval Underwater Systems Ctr.
Department of the Navy
Newport, RI 02840
Attn: D. J. Goodrich
        Code 3634
(Copy No. 10)

Commander
Naval Sea Systems Command
Department of the Navy
Washington, DC 20362
Attn: A. R. Paladino
        Code NSEA-55N
(Copy No. 5)

Commanding Officer
Naval Underwater Systems Ctr.
Department of the Navy
Newport, RI 02840
Attn: R. H. Nadolink
        Code 3634
(Copy No. 11)

Commander
Naval Sea Systems Command
Department of the Navy
Washington, DC 20362
Attn: W. D. Marlin
        Code NSEA-931E
(Copy No. 6)

Commanding Officer
Naval Underwater Systems Ctr.
Department of the Navy
Newport, RI 02840
Attn: C. N. Pryor
        Code 01
(Copy No. 12)

Commander
Naval Sea Systems Command
Department of the Navy
Washington, DC 20362
Attn: E. G. Liszka
        Code PMS-406B
(Copy No. 7)

Commanding Officer
Naval Underwater Systems Ctr.
Department of the Navy
Newport, RI 02840
Attn: C. Hervey
        Code 3634
(Copy No. 13)

Officer-in-Charge
David W. Taylor Naval Ship
Research & Development Ctr.
Department of the Navy
Bethesda, MD 20084
Attn: M. M. Sevik
Code 19
(Copy No. 14)

Officer-in-Charge
David W. Taylor Naval Ship
Research & Development Ctr.
Department of the Navy
Bethesda, MD 20084
Attn: J. H. McCarthy
Code 154
(Copy No. 15)

Officer-in-Charge
David W. Taylor Naval Ship
Research & Development Ctr.
Department of the Navy
Bethesda, MD 20084
Attn: T. T. Huang
Code 1552
(Copy No. 16)

Officer-in-Charge
David W. Taylor Naval Ship
Research & Development Ctr.
Department of the Navy
Bethesda, MD 20084
Attn: J. Shen
Code 194
(Copy No. 17)

Commander
Naval Surface Weapons Ctr.
Department of the Navy
Silver Spring, MD 20910
Attn: G. C. Guanaurd
(Copy No. 18)

Office of Naval Research
800 North Quincy Street
Department of the Navy
Arlington, VA 22217
Attn: R. Whitehead
Code 432
(Copy No. 19)

Office of Naval Research
800 North Quincy Street
Department of the Navy
Arlington, VA 22217
Attn: M. M. Reischman
Code 432F
(Copy No. 20)

Mr. P. S. Klebanoff
National Bureau of Standards
771.FM105
Washington, DC 20234
(Copy No. 21)

Mr. J. M. McMichael
National Bureau of Standards
771.FM105
Washington, DC 20234
(Copy No. 22)

Mr. R. J. Hansen
Naval Research Laboratory
Department of the Navy
Washington, DC 20390
(Copy No. 23)

Mr. R. King
Rand Corporation
1700 Main Street
Santa Monica, CA 90406
(Copy No. 24)

Mr. J. Aroesty
Rand Corporation
1700 Main Street
Santa Monica, CA 90406
(Copy No. 25)

Mr. C. Gazley
Rand Corporation
1700 Main Street
Santa Monica, CA 90406
(Copy No. 26)

Mr. A. R. Wazzan
Rand Corporation
1700 Main Street
Santa Monica, CA 90406
(Copy No. 27)

Mr. W. W. Haigh
Dynamics Technology, Inc.
22939 Hawthorne Blvd.
Torrance, CA 90505
(Copy No. 28)

Mr. G. L. Donohue
Dynamics Technology, Inc.
22939 Hawthorne Blvd.
Torrance, CA 90505
(Copy No. 29)

Prof. W. M. Phillips
Chairman
Dept. of Mech. Engr.
Purdue University
Lafayette, IN 47907
(Copy No. 30)

Dr. R. F. Mons
Westinghouse Electric Corp.
Post Office Box 1458
Annapolis, MD 21404
(Copy No. 31)

Prof. J. L. Lumley
Sibley School of Engineering
Cornell University
Ithaca, NY 14850
(Copy No. 32)

Prof. C. L. Merkle
Dept. of Mech. Engineering
The Pennsylvania State University
University Park, PA 16802
(Copy No. 33)

Mr. N. K. Madavan
Dept. of Mech. Engineering
The Pennsylvania State University
University Park, PA 16802
(Copy No. 34)

Director
Applied Research Laboratory
The Pennsylvania State University
Post Office Box 30
State College, PA 16804
Attn: ARL/PSU Library
(Copy No. 35)

Director
Applied Research Laboratory
The Pennsylvania State University
Post Office Box 30
State College, PA 16804
Attn: S. Deutsch
(Copies 36 through 38)

Director
Applied Research Laboratory
The Pennsylvania State University
Post Office Box 30
State College, PA 16804
Attn: G. B. Gurney
(Copy No. 39)

Director
Applied Research Laboratory
The Pennsylvania State University
Post Office Box 30
State College, PA 16804
Attn: R. E. Henderson
(Copy No. 40)

Director
Applied Research Laboratory
The Pennsylvania State University
Post Office Box 30
State College, PA 16804
Attn: L. R. Hettche
(Copy No. 41)

Director
Applied Research Laboratory
The Pennsylvania State University
Post Office Box 30
State College, PA 16804
Attn: B. R. Parkin
(Copy No. 42)

Director
Applied Research Laboratory
The Pennsylvania State University
Post Office Box 30
State College, PA 16804
Attn: GTWT Files
(Copy No. 43)